HHS Public Access

Author manuscript

Biochemistry. Author manuscript; available in PMC 2019 January 31.

Published in final edited form as:

Biochemistry. 2017 March 21; 56(11): 1604–1619. doi:10.1021/acs.biochem.6b00634.

Nuclear Magnetic Resonance Structures of GCN4p Are Largely Conserved When Ion Pairs Are Disrupted at Acidic pH but Show a Relaxation of the Coiled Coil Superhelix

Anne R. Kaplan[†], **Megan R. Brady**[†], **Mark W. Maciejewski**[‡], **Richard A. Kammerer**[§], and **Andrei T. Alexandrescu**[*,†]

[†]Department of Molecular and Cell Biology, University of Connecticut, Storrs, Connecticut 06269-3125, United States [‡]Department of Molecular Biology and Biophysics, UConn Health, Farmington, Connecticut 06030-3305, United States [§]Laboratory of Biomolecular Research, Division of Biology and Chemistry, Paul Scherrer Institut, 5232 Villigen-PSI, Switzerland

Abstract

To understand the roles ion pairs play in stabilizing coiled coils, we determined nuclear magnetic resonance structures of GCN4p at three pH values. At pH 6.6, all acidic residues are fully charged; at pH 4.4, they are half-charged, and at pH 1.5, they are protonated and uncharged. The α-helix monomer and coiled coil structures of GCN4p are largely conserved, except for a loosening of the coiled coil quaternary structure with a decrease in pH. Differences going from neutral to acidic pH include (i) an unwinding of the coiled coil superhelix caused by the loss of interchain ion pair contacts, (ii) a small increase in the separation of the monomers in the dimer, (iii) a loosening of the knobs-into-holes packing motifs, and (iv) an increased separation between oppositely charged residues that participate in ion pairs at neutral pH. Chemical shifts (HN, N, C′, Cα, and Cβ) of GCN4p display a seven-residue periodicity that is consistent with α-helical structure and is invariant with pH. By contrast, periodicity in hydrogen exchange rates at neutral pH is lost at acidic pH as the exchange mechanism moves into the EX1 regime. On the basis of ^{1}H–^{15}N nuclear Overhauser effect relaxation measurements, the α-helix monomers experience only small increases in picosecond to nanosecond backbone dynamics at acidic pH. By contrast, ^{13}C rotating frame T_1 relaxation ($T_{1\rho}$) data evince an increase in picosecond to nanosecond side-chain dynamics at lower pH, particularly for residues that stabilize the coiled coil dimerization interface through ion pairs. The results on the structure and dynamics of GCNp4 over a range of pH values help rationalize why a single structure at neutral pH poorly predicts the pH dependence of the unfolding stability of the coiled coil.

[*]**Corresponding Author**: Department of Molecular and Cell Biology, University of Connecticut, 91 N. Eagleville Rd., Storrs, CT 06269-3125. andrei@uconn.edu. Telephone: (860) 486-4414. Fax: (860) 486-4331.

Author Contributions

A.R.K. and M.R.B. contributed equally to this work.

Supporting Information

The Supporting Information is available free of charge on the ACS Publications website at DOI: 10.1021/acs.biochem.6b00634. GCN4p chemical shift differences between pH 6.6 and 1.5 (Figure S1), chemical shift periodicity due to the α-helical structure of α-synuclein (Figure S2), and simulations of the relationship between interchain NOE register and supercoiling (Figure S3) (PDF)

The authors declare no competing financial interest.

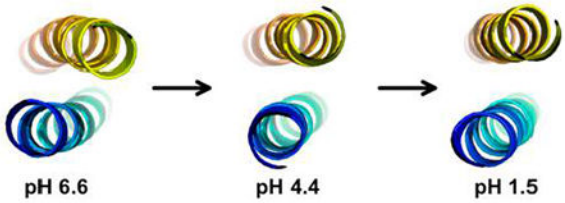

A principal advantage of NMR for structural studies is the ability to study molecules in solution[1] and to investigate how structure responds to changes in the environment. Thus, one could make “movies” of structures, where each frame corresponds to an incremental change in solution conditions. While NMR has become one of the main techniques for structure determination and there has been exciting progress in extending NMR methodology to ever larger and more complex macromolecules and assemblies,[2,3] the use of the technique to detail small structural changes is relatively unexplored. In X-ray crystallography, closely related structures can be determined routinely with the aid of molecular replacement and difference Fourier maps.[4] Analogous approaches in NMR have not yet been developed. Moreover, there is the issue of the level of precision needed for NMR to accurately model small structural changes.[2] The motivation for sampling structure under a variety of conditions is that to fully understand biological function it is often indispensable to have structural information about multiple conformational states.[5] For example, for rational drug design, it is useful to have models of both the free and ligand-bound receptor. To relate structure to stability, it helps to know how the structure responds to excursions from physiological conditions, such as the presence of denaturants, changes in temperature, or changes in pH. In particular, theoretical attempts to account for contributions to protein stability from the charging of ionizable residues have had only limited success, partially because structures are typically available at only one pH value.[6–8]

The GCN4p leucine zipper fragment of the yeast transcriptional activator GCN4 is a 33-residue coiled coil dimer (7.6 kDa) that has had its structure extensively determined and has been the subject of numerous biophysical studies.[9–17] Ion pairs, interactions between oppositely charged residues, are often seen in X-ray structures of coiled coils,[14,18,19] and mutagenesis of the charged residues can result in significant stability losses.[10,20] By contrast, the pK_a values of GCN4p, which have been completely determined by NMR in solution, predict only small contributions to stability from charge interactions.[8,12] Continuum electrostatic calculations of pK_a values in GCN4p, based on the X-ray structure of the coiled coil [Protein Data Bank (PDB) entry 2ZTA],[14] were used to model the experimentally determined pH dependence of stability to urea unfolding.[8] While the stability profile matched experiment near neutral pH, theoretical calculations overpredicted the destabilizing effects of the titration of ionizable residues at extremes of pH. The most likely source of error in the calculations is that they were based on a single structure of GCN4p at neutral pH, with no information about the nature of structural rearrangements that accompany changes in pH.[6–8] To the best of our knowledge, the only study to systematically address changes in structure accompanying changes in pH is a crystallographic study of ribonuclease A, which followed the titration of histidines at six pH values ranging from 5.5

to 8.8.[21] Structural changes included local changes around the histidines in the active site of the enzyme, as well as more distant concerted perturbations transmitted from His48 to the region near Glu101 by a network of hydrogen bonds (H-bonds).[21]

In this work, we examine the GCN4p coiled coil structure between neutral and acidic pH. Acidic rather than basic pH was chosen for these studies, because high pH leads to the loss of NMR signals from amide protons due to base-catalyzed exchange with solvent.[22] Guided by our complete determination of pK_a values for acidic and basic residues in GCN4p,[8] we chose three pH values for NMR structure determination. At pH 6.6, all of the acidic residues in the protein are charged, and ion pairs in the coiled coil are fully formed. At pH 4.4, near the pK_a values of the Asp and Glu residues (that cover a pH range between 4.6 and 3.5), the populations of charged and uncharged states are approximately equal. At pH 1.5, well below their pK_a values, the acidic residues are protonated and uncharged; therefore, all ion pairs in the coiled coil are broken. An analysis of Crick coiled coil parameters,[23] and of the knobs-into-holes packing[24] that is characteristic of coiled coils, was used to investigate perturbations of the quaternary structure of the homodimer. Distances between charged residues were analyzed to correlate side-chain structural changes with the breaking of ion pairs at low pH. We looked at the backbone dynamics of the coiled coil as a function of pH, using $^{1}H–^{15}N$ NOE relaxation data that probe fast motions on the fast picosecond to nanosecond time scale and ^{1}H to ^{2}H hydrogen exchange (HX) that is sensitive to motion on a slow time scale of hours or longer. Finally, differences in side-chain dynamics between near-neutral and acidic pH were investigated with rotating frame T_1 relaxation data ($T_{1\rho}$) for methylene ^{13}C nuclei in polar and nonpolar residues.

EXPERIMENTAL PROCEDURES

Materials.

Polymerase chain reaction was used to prepare a synthetic gene corresponding to residues Met250–Glu280 of GCN4 (NCBI accession number NP_010907), optimized for codon usage in *Escherichia coli*.[25] The cDNA fragment was ligated into the *Bam*HI/*Eco*RI sites of plasmid pHisTrx2, a derivative of pET-32a (Novagen), that encodes E. coli thioredoxin with an N-terminal His_6 tag and a thrombin cleavage site followed by a unique multiple-cloning site.[26] Freshly transformed *E. coli* JM109(DE3) cells were grown overnight in a 100 mL culture of LB medium and resuspended in 1 L of “new minimal medium”[27] supplemented with 1 g/L $^{15}NH_4Cl$ and 3 g/L [$^{13}C_6$]glucose. When the cells at 37 °C reached an OD_{600} of 0.6, expression of the His_6-thioredoxin-GCN4p fusion protein was induced with 1 mM IPTG for 4 h at 37 °C. Purification of the His6-Tagged fusion was achieved by affinity chromatography on Ni^{2+}-Sepharose (Novagen) under denaturing conditions. Thrombin cleavage of recombinant GCN4p from the His6-Tagged thioredoxin carrier was performed as described in the manufacturer’s instructions (Amersham). The purified GCN4p protein was dialyzed extensively against 10 mM NaCl and 10 mM sodium phosphate buffer (pH 6.2) using Biotech dialysis tubing (SpectraPor) with a 3.5 kDa molecular weight cutoff. Samples were lyophilized and stored at −20 °C.

For the sake of being consistent with previous studies, the sequence numbering scheme in this paper is the same as that for the 2ZTA X-ray structure of GCN4p.[14] The peptide in this

work, however, differs from that used for crystallography at two sites. At the N-terminus of our peptide, the two extraneous residues Gly0 and Ser1 substitute for Arg1 in the peptide for crystallography (Arg249 of GCN4), because of an engineered thrombin site used for protein purification. At the C-terminus of the peptide used for crystallography, residue Arg33 (Arg281 of GCN4) was omitted because it occurs in a heptad **d** position. The last two residues, Glu32 and Arg33 (amino acids Glu280 and Arg281 of GCN4, respectively), were not visible in the X-ray structure.[14]

NMR Spectroscopy.

NMR experiments were performed on samples containing 1.5 mM ^{13}C- and ^{15}N-labeled GCN4p monomer (0.75 mM dimer), 10 mM NaCl, and 10 mM sodium phosphate. A 600 MHz Inova NMR spectrometer equipped with a cryogenic probe was used to collect all NMR data at 25 °C, except for isotope-filtered NOE experiments, for which an 800 MHz spectrometer was used. Previously published ^{1}H, ^{13}C, and ^{15}N assignments for native GCN4p (BMRB accession code 15316)[8] were extended with three-dimensional (3D) HNCACB, HNCO, and CCH-TOCSY experiments recorded at each of the three pH values. Additional 200 ms mixing time 3D ^{15}N- and ^{13}C-edited NOESY-HSQC spectra at each pH value were used to obtain distance restraints for structure calculations. NMR data were processed using FELIX-NMR and analyzed using CCPNmr Analysis.[28] The standard DSS (2,2-dimethyl-2-silapentane-5-sulfonate) was used as an internal ^{1}H chemical shift reference, while ^{13}C and ^{15}N shifts were referenced indirectly as described in the literature.[29] Chemical shift deviations from random coil values were calculated as (observed-coil), using published random coil reference values.[30] NMR assignments for GCN4p have been deposited with the following BMRB accession codes: 30027 for pH 6.6, 30028 for pH 4.4, and 30029 for pH 1.5.

To identify NOE distance contacts between chains in GCN4p, we prepared a mixed dimer consisting of ^{13}C and ^{12}C monomers. Samples of natural abundance [^{12}C]GCN4p and isotopically enriched [^{13}C]GCN4p were mixed in 6 M urea, conditions under which the protein is an unfolded random coil. To remove urea, the mixed sample was dialyzed with a 3.5 kDa cutoff filter, once against 1 M NaCl and three times against 10 mM NaCl and 10 mM sodium phosphate. Analysis of the ratio of NMR signals from [^{12}C]GCN4p to the doublets that result from $^{1}J_{H-^{13}C}$ splitting in [^{13}C]GCN4p, using assigned aromatic resonances in the one-dimensional (1D) ^{1}H NMR spectrum, showed that the ^{13}C:^{12}C GCN4p ratio was 2:1, corresponding to a concentration of the mixed [^{12}C/^{13}C]GCN4p dimer of ~0.25 mM in the sample that had a total dimer concentration of 0.75 mM. To identify interchain NOEs, 200 ms mixing time sensitivity-enhanced 3D ^{13}C-F1-filtered, ^{13}C-F3-edited NOESY-HSQC experiments from the Varian Protein Pack were performed at each of the three pH values. The ^{13}C-filtered NOESY-HSQC experiments were performed at 25 °C on an 800 MHz Inova NMR spectrometer operating with a cryogenic probe. The sensitivity of the ^{13}C-filtered NOESY experiments was low compared to that of a test sample of ^{12}C/^{13}C mixed CMPcc, a trimeric coiled coil from cartilage matrix protein.[31] Because of the low sensitivity, each ^{13}C-filtered NOESY spectrum on the [^{12}C/^{13}C]GCN4p mixed dimer sample was acquired for 6.5 days at 800 MHz. Only off-diagonal peaks were included in the analysis of NOE contacts. Diagonal peaks, even when corresponding to

possible legitimate interchain contacts (e.g., $V23^A$ Hγ2 methyl—$V23^B$ Hγ2 methyl), were omitted because these could have been caused by leak-through of large signals through the ^{13}C isotope filter.

Calculation of NMR Structures.

NMR structures of GCN4p at the three pH values were calculated from the experimental restraints summarized in Table 1. Backbone Φ and Ψ and side-chain χ_1 dihedral angles were obtained from assigned H, HN, Hα, Cα, Cβ, and C′ chemical shifts with TALOS-N.[32] Intramonomer distance restraints at each pH value were obtained from ^{15}N- and ^{13}C-edited NOESY-HSQC spectra. Interchain distance restraints were from the ^{13}C-filtered NOESY-HSQC spectra. Regular α-helix C′(i)–NH(i + 4) H-bond restraints were included for residues 5–30 at pH 6.6, because all of these are involved in H-bonds in the 2ZTA X-ray structure. The same H-bonds were included for the pH 4.4 structure because all amide protons from this region that were resolved in the NMR spectrum showed protection from hydrogen exchange (HX). At pH 1.5, 10 H-bond restraints were excluded for residues 7, 11, 13, 15–18, 20, 21, and 28, because their amide proton showed no HX protection. As a test, we also calculated a set of pH 1.5 structures with all H-bonds included for residues 5–30, like for the pH 6.6 and 4.4 structures. No large differences were seen for the structures when the 10 H-bonds were omitted at pH 1.5, because the NOE and dihedral restraints are sufficient to constrain the 10 residues without protected amide protons in α-helical conformations.

NMR structures were calculated with a distance geometry/simulated annealing protocol using X-plor NIH (version 2.40).[33] Noncrystallographic symmetry (NCS) restraints were used in the calculations,[31] as NMR spectra indicate that the two monomers in the symmetric dimer are magnetically equivalent. With 200 initial structures with randomized ϕ and ψ dihedral angles as the starting point, the 20 lowest-energy structures with no NOE violations of >0.3 Å or dihedral angle violations of >4° were kept for analysis. Of the 20 structures from X-plor, the most representative of the ensemble average was selected as a starting structure for water refinement of 45 structures with ARIA.[34] NCS restraints were included in the water refinement, and the molecular topology file was used to keep Asp and Glu residues charged at pH 6.6 but uncharged at pH 4.4 and 1.5. In separate tests, the charge state of the Asp and Glu residues was found to make little difference to the structures. The 20 lowest-energy structures from the ARIA[34] water refinement protocol were selected as the final structures. These had no NOE violations of >0.4 Å and no dihedral angle violations of >5°. The final NMR structures (Table 1) have been deposited in the Protein Data Bank as entries 5IEW (pH 6.6), 5IIR (pH 4.4), and 5IIV (pH 1.5). Structure “1” of each ensemble is the one closest to the NMR ensemble mean.

Structure Analysis.

Structures were visualized and analyzed with PyMol.[35] The program was also used to superimpose structures and calculate RMSDs using the “Align” function, as well as to calculate distances between charged residues. Coiled coil parameters were calculated using the Coiled Coil Crick Parameterization (CCCP) server (http://www.grigoryanlab.org/cccp).[23]

Knobs-into-holes packing of coiled coil structures was characterized using the SOCKET server (http://coiledcoils.chm.bris.ac.uk/socket/server.html).[24]

Hydrogen Exchange.

Hydrogen exchange (HX) experiments were performed at pH 4.4 and 1.5 and a temperature of 10 °C, for comparison with previously published data recorded at pH 7.0 and 10 °C.[11] To initiate HX, ^{15}N-labeled GCN4p was dissolved to a monomer concentration of 1.5 mM in 99.96% D_2O. Decays of ^{1}H–^{15}N HSQC cross-peak intensities as a function of D_2O incubation time were fitted to single exponentials, to calculate HX lifetimes and their associated uncertainties.[36]

NMR Relaxation Experiments.

Backbone dynamics on the picosecond to nanosecond time scale were characterized with ^{1}H–^{15}N NOE relaxation data measured at 600 MHz and 25 °C. The ^{1}H-^{15}N NOE data were obtained from spectra in which the proton signals were saturated for 3 s and control experiments in which the saturation period was replaced with an equivalent preacquisition delay. ^{1}H–^{15}N NOE values and their associated uncertainties were calculated as previously described.[37]

Side-chain dynamics were investigated by measuring $T_{1\rho}$ values for methylene carbons in samples of 1.5 mM ^{13}C-labeled GNC4p dissolved in 99.96% D_2O, at pH 6.6 and 1.5. The $T_{1\rho}$ spectra were recorded at 600 MHz and 25 °C, with an experiment from the Varian Protein pack. A preacquisition delay of 2 s was used, and eight $T1_{\rho}$ relaxation times of 10, 40, 70, 100, 130, 160, 190, and 250 ms were sampled. $T_{1\rho}$ time constants were obtained from exponential fits of decays in ^{1}H–^{13}C cross-peak intensities with relaxation time. Uncertainties were taken as the standard errors of the fits.

RESULTS

Chemical Shifts Are Consistent with GCN4p Retaining α-Helical Structure at Acidic pH.

Figure 1 shows assigned ^{1}H–^{15}N HSQC spectra of GCN4p at the three pH values used for structure determination. The spectra have a single set of NMR resonances corresponding to the amino acid sequence of the monomers, indicating that the peptide chains are magnetically equivalent because of the 2-fold symmetry of the coiled coil homodimer. There are changes in ^{1}H and ^{15}N shifts between pH 6.6 and 1.5 (Figure 1A,C); a chemical shift difference plot (Figure S1) indicates that most of the differences occur near the ionizable Glu residues that titrate with pH and the basic Arg and Lys residues that can ion pair with them.

Figure 2 shows plots of chemical shift differences between GCN4p and random coil values. The HN (Figure 2A) and N (Figure 2B) shifts show average chemical shift differences near zero. By contrast, the C′ and Cα atoms (Figure 2C,D) show overall positive differences and the Cβ atoms (Figure 2E) negative differences that are all consistent with α-helical secondary structure.[30] As previously reported,[11] the HN resonances show a periodicity where heptad repeat positions a and e show large downfield shifts (positive differences) and

positions **b** and **f** large upfield shifts (Figure 2A). The N resonances show a periodicity where **g** positions have large values and **b** positions have small values (Figure 2B). The periodicity of C′ nuclei gives large shift differences for *c* positions and smaller values for *a* and *d* positions (Figure 2C). The periodicity of C′ chemical shift differences has been previously noted for another coiled coil.[38] For the Cα and Cβ chemical shift differences, we see increased chemical shift differences for heptad positions **a** and **d**, respectively (Figure 2D,E). To the best of our knowledge, the chemical shift periodicity for N, Cα, and Cβ nuclei has not been previously described.

The chemical shift periodicity for the HN resonances is correlated with the lengths of backbone NH…OC′ H-bonds in the 2ZTA structure.[11,14] The H-bond lengths vary because of the alternating pattern of hydrophobic and hydrophilic residues in the α-helix, which bends the α-helix monomers to form the supercoil in the coiled coil.[39] The fact that the periodicity patterns seen for different types of nuclei such as HN, N, C′, Cα, and Cβ are different suggests that except for HN signals, the chemical shift periodicity is not related to H-bond length but is a feature of α-helix secondary structure. A periodic variation of H-bond lengths along the length of an α-helix, and the ensuing bending, is not unique to coiled coils but also occurs in regular α-helices.[40] Thus, at least for HN chemical shifts, a seven-residue periodicity identical to that observed in coiled coils is seen for regular α-helices in the micelle-bound states of the peptides mastoparan[41] and amylin.[42] To test the extent to which the chemical shift periodicity observed for GCN4p (Figure 2) is a generic feature of α-helices, we examined the SLAS micelle-bound state of monomeric α-synuclein, for which comprehensive NMR assignments are available (BMRB entry 16302).[43] We found a similar albeit weaker periodicity pattern as seen for GCN4p (Figure 2) for the HN, C′, and Cα signals of the first 40 of ~90 residues that adopt an α-helix structure in the micelle-bound state of α-synuclein (Figure S2). Only the N nuclei appear to have a seven-residue periodicity that is shifted by three sequence positions compared to that of the coiled coil (Figure S2). The periodicity pattern can be extended to residue ~70, if it is assumed that there is a two-residue sequence insertion near residue 40, probably a consequence of a kink or a bend in this region of the α-synuclein helix. The pattern can be further extended to residue ~85 if another one-residue insertion is allowed at position 77. The fact that the chemical shift periodicity seen for GCN4p whose sequence is based on heptad repeats is similar to that observed for α-synuclein that has a sequence based on 11-residue repeats strongly suggests that these patterns are characteristic of α-helical structure rather than a specific feature of coiled coils. Further support for this hypothesis comes from our analysis of chemical shift deviations from random coil values in the X form of GCN4p (BMRB entry 5744),[13] which is likely to be an α-helix monomer rather than a dimer. The chemical shift periodicity of the reported HN, N, and Cα nuclei[13] is conserved in heptad repeats 1 and 3 but breaks down for heptad repeat 2, which has a lower fractional population of α-helix.[13] It is only the Cβ nuclei that appear to be sensitive to whether the GCN4p polypeptide is in an α-helical monomer or a coiled coil dimer.[13]

Chemical shift differences from random coil values for the HN, N, C′, Cα, and Cβ nuclei of GCN4p as well as their sequence periodicities are highly conserved between pH 6.6 and 1.5

(Figure 2). This strongly suggests that the α-helical secondary structure of the GCN4p dimer is retained from neutral pH to acidic solutions as low as pH 1.5.

Structure Determination of GCN4.

To gain insight into the structural changes accompanying acidification, we determined NMR structures of GCN4p at pH 6.6, 4.4, and 1.5. Structure calculations were based on dihedral angle restraints calculated from chemical shifts using TALOS-N,[32] hydrogen-bond restraints for protected amide protons, and distance restraints from 3D ^{15}N- and ^{13}C-edited NOESY-HSQC spectra. A problem that arises for structure determination of symmetric oligomers, in which the monomers are magnetically equivalent, is distinguishing NOE distance contacts within a monomer from those between monomers. Although many symmetric oligomer NMR structures have been determined using an ambiguous restraint strategy,[44] we thought we could get more equivocal results for GCN4p by directly measuring interchain NOEs using a ^{13}C-filtered NOESY experiment that transfers magnetization only from protons on ^{12}C monomers to protons on ^{13}C monomers, in dimers formed from a mixture of ^{12}C and ^{13}C chains.[31,45] Figure 3A shows the aromatic region of a 1D ^{1}H NMR spectrum of the GCN4p ^{12}C/^{13}C mixed dimer sample prepared by combining the chains under denaturing conditions and refolding the protein by dialysis of the urea denaturant. Each of the four aromatic signals from GCN4p shows a triplet, where the inner component (solid line) corresponds to protons attached to ^{12}C chains and the outer components (dashed lines) correspond to protons attached to ^{13}C, which are split by the one-bond $^{1}J_{HC}$ coupling. Figure 3B compares a ^{13}C-edited 1D spectrum (bottom) with the first FID of the 3D ^{13}C-F1-filtered, ^{13}C-F3-edited NOESY-HSQC experiment (top). Most of the NOE signal in the top spectrum comes from the methyl region between 0.8 and 1.0 ppm, consistent with the coiled coil dimerization interface being comprised of methyl groups from hydrophobic Leu and Val residues.

It is evident from the top spectrum that the efficiency of NOE transfer in the 1D ^{13}C-filtered NOESY experiment is poor. To obtain acceptable sensitivity, it was necessary to collect the 3D ^{13}C-F1-filtered, ^{13}C-F3-edited NOESY-HSQC spectra for 6.5 days at 800 MHz, at each of the three pH values. Figure 3C compares representative ^{1}H–^{1}H NOESY strips at the indicated ^{13}C planes from the 3D ^{13}C-filtered NOESY experiments at the three pH values. The strips for the Val30 Hα proton, showing NOEs to the Val30 Hγ2 methyl group on the opposite chain, are representative of the majority of interchain contacts that are unchanged with pH. By contrast, the Met2 Hε methyl group shows interchain NOEs to the Leu5 Hδ methyl that are conserved with pH, but a number of other NOEs at pH 6.6 to Ser1, Met2, and Lys3 on the opposite chain disappear at low pH. Finally, the Lys27 Hε methylene protons show NOEs to the Leu26 Hδ1 methyl and Glu22 Hβ1 protons from the opposite chain, with the latter NOE likely due to the Lys27–Glu22 interchain salt bridge. The NOE to the Glu22 Hβ1 proton is lost below pH 6.6, while those to the Leu26 Hδ1 methyl group decrease with a lowered pH. Both observations are likely to be a manifestation of the disruption of the Lys27–Glu22 interchain salt bridge at acidic pH.

Structures of GCN4p as a Function of pH.

The NMR structures of GNC4p at pH 6.6, 4.4, and 1.5 are shown in Figure 4. Statistics for the NMR structures are listed in Table 1. For calibration, we compared the NMR structures to a set of six X-ray structures of GCN4p shown in Figure 4A. The X-ray structures were selected because they did not have large sequence changes compared to that of WT GCN4p; they were not linked to large cofactors or proteins that could perturb the coiled coil, and the crystals were grown over a range of pH values (from 8.5 to 6.0) near neutrality.

The NMR structures at pH 6.6 (Figure 4B) are very similar to the X-ray structures of GCN4p near neutral pH (Figure 4A). The main difference is that surface polar side chains show greater conformational variability in the solution NMR structures compared than the X-ray crystallography set does (Figure 5). This is typical of other proteins when their NMR and X-ray structures are compared.[46] By contrast, the side chains of the **a** and **d** heptad positions that make up the hydrophobic core of the coiled coil are well-defined and show similar rotameric states (Figure 4A,B), except for N16, which exists in two conformations in the X-ray structure.[14]

The RMSDs between the pH 6.6 NMR structures and the prototypical 2ZTA X-ray structure of GCN4p are 0.79 and 1.04 A for the backbone and all heavy atoms, respectively (Table 1). It is worth noting that because of crystal lattice packing distortions, the two polypeptide chains in the 2ZTA X-ray structure are not identical. Thus, chains A and B of the 2ZTA X-ray structure differ with backbone and heavy atom RMSDs of 0.63 and 1.40 Å, respectively. The variation within the set of six X-ray structures (Figure 4A) is similar albeit smaller than that between the two chains of the 2ZTA X-ray structure, with RMSDs of 0.26 and 0.34 Å for backbone and all heavy atoms, respectively. The fact that the structural agreement is better among the set of six X-ray structures than between two chains of a single X-ray structure could be a consequence of GCN4p crystallizing in the same C_{121} space group in all six cases. Thus, the structures of the A and B monomers would be subject to the same lattice packing perturbations in all six crystallographic structures.

As the pH is lowered to 4.4 (Figure 4C) and 1.5 (Figure 4D), there is a small but systematic decrease in the precision of the NMR structures compared to that at pH 6.6 (Figure 4B). Additionally, the NMR structures diverge from the pH 6.6 NMR structures and from the 2ZTA X-ray structure with a decrease in pH (Table 1). The RMSD between the neutral and acidic pH structures is larger and increases faster with pH for the coiled coil dimer than for the individual α-helix monomers (Table 1). This suggests that the principal structural changes at low pH involve differences in the packing of the dimers rather than changes in the α-helix monomer structures. This is most apparent as a slight movement apart and a decreased extent of winding of the two α-helices around each other at low pH (Figure 4B–D).

Acidic pH Causes Unwinding of the GCN4p Superhelix.

To obtain a quantitative description of the changes in the GCN4p structure with a decrease in pH, we analyzed the three sets of NMR structures using the CCCP (Coiled Coil Crick Parameterization) program.[23] The program fits α-helices in superstructure to mathematical

parameters for an idealized coiled coil developed by Crick.[47] The subset of these parameters used in our analysis is illustrated in Figure 4E, and the average values in different GCN4p structures are listed in Table 2.

Parameters R_1 and R_0 refer to the radii of α-helix monomers and of the supercoil in the dimer, respectively (Figure 4E). α-Helix radius R_1 fluctuates between 2.1 and 2.2 Å, with little difference from the 2.1 Å mean in the set of X-ray structures (Table 2). Thus, the radii of the α-helix monomers are conserved as a function of pH and between the NMR and X-ray structures. R_0, which is related to the distance between the axes of the two α-helices in the dimer, shows a small but systematic increase of 0.2 Å between pH 6.6 and 1.5, indicating that the α-helices are moving slightly apart at acidic pH (Table 2). The X-ray structures have an R_0 larger than that of the NMR structures at any pH. This discrepancy could be due to differences between the solution and the crystals or a systematic offset in the calibration of intermolecular NOEs, so that the increase in R_0 with a decrease in pH within the set of NMR structures is likely to be genuine.

ω_1 and ω_0 refer to the frequencies, or the degrees of twist, of the α-helices and the supercoil, respectively (Figure 4E). ω_0 is the angle the superhelix turns around the coiled coil axis for each residue, and ω_1 is the corresponding parameter for the turn per residue around the α-helix axis. Both parameters appear to show systematic changes with a decrease in pH (Table 2). An analysis of a database of ~860 coiled coil structures showed that the ω_0 parameter in left-handed coiled coils ranges from 0 for parallel helices to −8.7 for the most tightly wound coiled coils, with the negative sign indicating a left-handed superhelix.[23] The mean value of ω_0 for this database was −3.5° per residue. Thus, a complete 360° turn of the superhelix occurs for an average value of 360/3.5 = 103 residues. For the pH 6.6 NMR structures, the ω_0 value of −4.8° per residue indicates that a complete turn of the superhelix occurs over 75 residues. For the pH 1.5 NMR structures, the ω_0 of −2.7° per residue implies 133 residues are needed for a turn of the superhelix, corresponding to an increase of ~75% compared to that at pH 6.6. On the basis of the NMR structures, the superhelix unwinds with a decrease in pH. It is interesting to note that the ω_0 of −3.8° per residue for the set of X-ray structures near neutral pH is larger than the average of −4.8° per residue for the pH 6.6 NMR structures (Table 2). Thus, under similar conditions near neutral pH, the pH 6.6 NMR structures appear to be more tightly wound than the X-ray structures. A possible source of this difference is that crystal lattice packing contacts may stretch the coiled coil structure or sterically occlude the winding of α-helices in the crystal compared to the solution state. Another possibly significant factor is that the peptide used for the NMR structures has differences at the N- and C-termini from those used for crystallography (described in Experimental Procedures), which may affect supercoiling.

ω_1, the turn per residue in an α-helix, has idealized values of 360/3.6 = 100.0° per residue for regular α-helices and 360/3.5 = 102.8° per residue for a left-handed coiled coil because of the hydrophobic packing constraints imposed by the seven-residue heptad repeat sequence. In the GCN4p X-ray structures and in the pH 6.6 NMR structures, the ω_1 values are close to the 102.8° per residue ideal of a coiled coil. As the pH is decreased, there is a decrease in ω_1 toward the 100.0° per residue limit of a regular α-helix (Table 2). It has been noted[23] that for the database of ~860 coiled coil structures ω_1 is anticorrelated to ω_0 (R =

−0.7). We see a similar inverse correlation ($R = -0.9$) for the rather limited data set of three pH points in the study presented here. The changes in ω_1 with a decrease in pH are small and only slightly larger than the spread of values within the NMR ensemble at each pH. Nevertheless, the small decreases in ω_1 are consistent with the loosening of the coiled coil superhelix exemplified by the more substantial increases in ω_0 as the pH is decreased.

In addition to the parameters given above, we looked at the rise per residue, *d*, which is close to the ideal value of an α-helix of 1.5 Å/residue and shows no change with pH. Z_{off}, the axial offset between equivalent positions in the α-helix monomers, fluctuates randomly near zero, as expected for a parallel coiled coil that maintains its 2-fold symmetry, demonstrated by magnetically equivalent monomers in the NMR spectra.

Finally, we examined side-chain packing in the GCN4p structures with SOCKET.[24] Coiled coils exhibit characteristic “knobs-into-holes” side-chain packing interactions. The knob formed by a heptad **a** position is surrounded by a diamond of holes comprised of $\mathbf{d}_{-1}\mathbf{g}_{-1}\mathbf{ad}$ positions from the opposite helix, where the subscript ±1 indicates positions in neighboring heptads.[24] Similarly, a **d** knob is surrounded by holes formed by residues $\mathbf{adea}_{+1}$. Using a default 7.0 Å packing distance cutoff, the SOCKET program identifies seven knobs-into-holes units per chain in the 2ZTA X-ray structures. Designated by the knobs, they are $L5^d$, $V9^a$, $L12^d$, $N16^a$, $L19^d$, $V23^a$, and $L26^d$ (the superscript indicates the heptad position). All of the knobs-into-holes units above are conserved in the pH 6.6 NMR structure. For the pH 4.4 structure, only the C-terminal $L26^d$ unit is lost, while for the pH 1.5 NMR structure, the N-terminal $L5^d$ unit is lost. With a tighter packing distance cutoff of 6.0 Å, all seven of the knobs-into-holes units survive in the pH 6.6 structures, but only four persist in the pH 4.4 and 1.5 structures. The units that are lost in each case are those closest to the ends of the polypeptide chain. Thus the knobs-into-holes packing of the GCN4p dimer is retained across the pH range studied, indicating the coiled coil structure is maintained. There is, however, a loosening of the dimer interface for the N-and C-terminal ends at low pH, concomitant with the relaxation of the coiled coil superhelix.

Acidic pH Disrupts Ion Pairs in the NMR Structures.

Because the changes in the GCN4p structures are associated with pH, we wanted to see the extent to which charge–charge interactions are involved. Parallel dimeric coiled coils have the potential to form intrahelical ion pairs between oppositely charged residues with an *i*, *i* + 3 or *i*, *i* + 4 sequence spacing because of the periodic nature of α-helical structure, as well as intermolecular ion pairs between residues with an *i*, *i* + 5′ sequence spacing particularly involving heptad repeat positions **e** and **g**.[8,12,48,49] There are five potential ion pairs in GCN4p (Table 2): three are intramolecular (E11–K8, E11–K15, and E22–R25), and two are intermolecular (E20-K15′ and E22–K27′). Four of the five potential ion pairs are observed as hydrogen-bonded salt bridges in the 2ZTA X-ray structure of GCN4p, but none are replicated on both chains of the 2-fold symmetric dimer. Moreover, the salt bridges in the 2ZTA structure are poorly conserved between GCN4p structures (Figure 5A). For example, the intramolecular E22–R25 interaction seen on chain A of the 2ZTA structure is observed on chains A of the 1ZIK, 1ZIL, and 4TL1 structures but not on either chain of the 1ZII or 2AHP X-ray structure. If we calculate closest approach distances between oppositely

charged moieties for both chains in the set of GCN4p X-ray structures, the average values are more consistent with long-range ion pair interactions than with H-bonded salt bridges that have to satisfy a heavy atom distance cutoff of 3.5 Å (Table 2). Alternatively, if we consider hydrogen-bonded salt bridge interactions, these occur in only a fraction of the X-ray structures (percent values in parentheses in Table 2).

The two intermolecular E20–K15′ and E22–K27′ ion pairs form hydrogen-bonded salt bridges in 55 and 20% of the NMR structures at pH 6.6, respectively, fractional populations similar to those in the X-ray set (Table 2). The proximity between these residues at pH 6.6 is supported by intermolecular NOEs between the side chains of E22 and K27 (Figure 3C) and E20 and K15 (not shown) that disappear at lower pH values. With decreasing pH, the closest contact distances between oppositely charged atoms in the two intermolecular ion pairs increase to values of >7 Å (Table 2), which are probably too large to support electrostatic interactions. Thus, the two intermolecular ion pairs appear to be present in solution at pH 6.6 but are disrupted at lower pH values when the acidic glutamate residues become neutralized. The two intermolecular ion pairs bring together residues at nonequivalent positions in the sequence across the dimer interface. This should favor supercoiling of the structure, whereas at low pH, the loss of these relatively long-range intermolecular contacts could contribute to the partial unwinding of the supercoil.

Of the three possible intramolecular ion pairs, the E11–K15 pair is not seen in the NMR or X-ray structures (Table 2), making it unlikely that a charge interaction between these residues occurs. Because of severe crowding of the lysine and glutamate side-chain resonances in the ^{13}C NOESY spectra, we were unable to detect intramolecular NOEs that support the E11–K8 or E22–R25 ion pairs. The E22–R25 side chains, however, are within ion pairing distance across the entire pH range (Table 2). Thus, the residues are fixed in proximity by the rest of the structure, in spite of the absence of direct distance constraint data. The E22–R25 pair forms intramolecular hydrogen-bonded salt bridges in 50% of the NMR structures at pH 6.6, a fractional population comparable to that seen for the X-ray set (Table 2). Although short side-chain distances for the E22–R25 pair persist in the lower-pH structures, the residues no longer maintain orientations compatible with hydrogen bonding at acidic pH. The possible E11–K15 ion pair gives uniformly large distances of >7 Å in the NMR structures at all three pH values. We cannot exclude the presence of this ion pair, however, because NMR spectral crowding may have obscured NOE distance contacts that support an interaction between the residues.

At low pH, there is also the potential for basic residues R25–K27 to participate in a repulsive charge-charge interaction. The average distances between R25 and K27, however, are >7 A in the NMR structures at all pH values, making it unlikely that this repulsive interaction plays a role in the structure. In summary, the ion pair analyses suggest that pH-dependent changes in the NMR structures of GCN4p are linked to the disruption of the intermolecular E20–K15′ and E22–K27′ interactions and the intramolecular E22–R25 interaction. The E11–K8 interaction could not be characterized, while attractive E11–K15 and repulsive R25–K27 interactions do not appear to occur.

How Disruption of Intermolecular Ion Pairs Leads to Superhelix Unwinding.

The differences in the NMR structures going from near-neutral to acidic pH include an increased separation between oppositely charged residues in ion pairs and an increase in the average value of superhelix parameter ω_0, implying a partial unwinding of the coiled coil. We wanted to test if the loss of superhelicity at low pH was due to a decrease in the precision of the pH 1.5 structures, because these are constrained by a smaller number of NOEs. To this end, we cross-validated the pH 6.6 structures against the pH 1.5 restraints and the pH 1.5 structures against the pH 6.6 restraints. In each of the cross-validation tests, ~10% of the NOEs gave violations of >0.5 Å. The dihedral angles showed fewer violations, with 0–3% of restraints being violated by more than 5°, because GCN4 maintains its α-helical secondary structure between pH 6.6 and 1.5. The largest distance violations on the order of 3–6 Å predominantly involved the charged residues that participate in ion pairs at neutral pH. For example at pH 1.5, the Hε proton of K15 gives an interchain NOE to the L13 methyl Hδ2 protons that is not seen at pH 6.6. Similarly, the E22 HN proton gives an intrachain NOE to the L19 Hδ1 methyl group only at pH 1.5. Presumably, these NOEs are lost because of the rearrangements that accompany the interchain K15–E20′ ion pair interaction at pH 6.6. The cross-validation analysis shows that the NMR structures at pH 6.6 and 1.5 are distinct, rather than the lower-pH structure corresponding to a less precise version of the high-pH structure. The changes in NOEs for the charged residues with pH need not correspond to the difference in superhelicity between the structures but could result from localized rearrangements of the charged side chains.

We hypothesized that the interchain E20–K15Å and E22–K27′ ion pairs favor a more negative superhelix frequency w_0, because they bring together residues in nonequivalent sequence positions. The distance contacts for the E20–K15′ and E22–K27′ ion pairs at pH 6.6 have the largest sequence separation among the interchain NOEs, where $i^A - j^B = 5$, where i^A is the sequence position of the first residue in chain A and j^B is the position of the second residue in chain B. In the pH 6.6 data set, there are seven additional NOEs for which $i^A - j^B = 4$ and six for which $i^A - j^B = 3$. The 39 remaining interchain NOEs at pH 6.6 are between residues on opposite chains that are separated by zero to two positions in the sequence ($2 \geq i^A - j^B = 0$). The numbers of both long-range and short-range interchain NOEs decrease in the pH 1.5 data set. At pH 1.5, there are no NOEs for which $i^A - j^B = 5$ as the interchain ion pair interactions are lost, five NOEs for which $i^A - j^B = 4$, four for which $i^A - j^B = 3$, and 26 short-range NOEs for which $2 \geq i^A - j^B = 0$. To test the hypothesis that the superhelix frequency depends on the register of the interchain distance contacts, we performed structure calculations with simulated data sets excluding NOEs with different $i^A - j^B$ values. The calculations were performed with the X-plor NIH program, without the water refinement step used for the final structures. For each simulation, 100 structures were calculated, and the 10 lowest-energy structures without NOE violations of >0.5 Å and dihedral violations of >5° were analyzed (Figure S3). Using the entire pH 6.6 restraint set, we obtained a mean superhelix frequency ω_0 of −4.6° per residue (Figure S3), comparable to the value of −4.8° per residue for the pH 6.6 structures after water refinement (Table 2). Excluding just two NOEs with the largest register number $i^A - j^B = 5$, due to the E20–K15′ and E22–K27′ ion pairs at pH 6.6, changed the superhelix frequency to −3.7° per residue. Further removing the seven interchain NOEs for which $i^A - j^B = 4$ from the pH 6.6 restraint

set increased ω_0 to −2.9° per residue, and additionally, excluding the six $i^A - j^B = 4$ interchain NOEs gave an ω_0 of −3.2° per residue. Thus, the supercoiling of the coiled coil is predominantly favored by interchain NOEs between residues with a large difference in sequence position. As a control, we performed a simulation in which we randomly removed half of the 39 short-range interchain NOEs with an $i^A - j^B$ index between 0 and 2 but kept the NOEs for which $i^A - j^B > 2$. In this control, ω_0 was −4.3° per residue, a value comparable to that using the full pH 6.6 restraint set. In a final test, we supplemented the pH 1.5 restraint set with the two interchain K15(ε)–E20(Hγ) and E22(Hβ1)–K27(Hε) ion pair NOEs from the pH 6.6 restraint set. We obtained 10 conformers with no restraint violations in this simulation, indicating the structures could converge to solutions that satisfied both the pH 1.5 restraints and the two artificially introduced long-range restraints from the pH 6.6 data set. ω_0 changed from −2.0° per residue with the pH 1.5 restraints alone to −2.7° per residue when the two $i^A - j^B = 5$ NOEs due to the interchain E20–K15′ and E22–K27′ ion pairs were added. The superhelix became more wound when the two long-range contacts from the pH 6.6 restraint set were included but not as much as in the pH 6.6 structures, because the restraints were specific to the pH 1.5 data set.

Taken together, the results of the simulations show that superhelix frequency parameter ω_0 becomes more positive as the number of long-range interchain distance contacts decreases. The pH 1.5 structure is unwound compared to that at pH 6.6, not solely because of an overall decrease in structural precision but because of the specific loss of the E20–K15′ and E22–K27′ interchain ion pairs at low pH. Conversely, the interchain ion pairs constrain residues with a relatively large $i^A - j^B = 5$ sequence separation across the dimer interface, leading to a greater superhelical twist at pH 6.6. The changes in ω_0 when the two interchain ion pair NOEs are removed are not as large as the difference between the pH 6.6 and 1.5 structures calculated with the full complement of restraints. This suggests that factors other than the interchain ion pairs are involved. As previously noted, the knobs-into-holes packing characteristic of coiled coils is largely maintained between neutral and acidic pH, but the packing is looser in the pH 1.5 structures particularly at the chain termini. The disruption of inter- and intrachain ion pairs at low pH could indirectly affect the knobs-into-holes packing interface, which may in turn also contribute to the unwinding of the coiled coil at low pH.

Hydrogen Exchange in GCN4p Is Dominated by Localized Dynamics.

Goodman and Kim[11] measured HX for GCN4p at pH 7 (Figure 6A) and noticed periodicity in the data similar to that for HN chemical shifts (Figure 1A). To aid visualization, the HX data for GCN4p in Figure 6 are expressed as exchange lifetimes, the inverse of the rate of exchange ($\tau = 1/k_{ex}$).[50] At pH 7, residues in heptad positions **a**, **d**, and **e** show strong HX protection while those in positions **c** and **f** show weak protection (Figure 6A). The protected amides are sheltered from solvent because they lie at the bottoms of the “holes”, into which the hydrophobic knobs from positions **a**′ and **d**′ of the other α-helix are packed. By contrast, amide protons in positions **c** and **f** are farther from the dimer interface and more exposed to solvent, leading to weaker HX protection.11

To examine the effects of pH, we measured HX in GCN4p at pH 4.4 (Figure 6B) and pH 1.5 (Figure 6C). In contrast to the data at pH 7, HX protection shows no discernible periodicity

at pH 4.4 or 1.5. The exchange lifetimes of the protected amide protons at acidic pH are also more uniform than at pH 7.0. The differences in HX could arise from changes in the structure at low pH or an increase in dynamics that overshadows the variation in protection observed at neutral pH. The latter explanation is more likely. HX is base- and acid-catalyzed, so that exchange lifetimes above a maximum near pH ~5 should decrease by a factor of 10 for every change of 1 pH unit.[51] The observed decrease between pH 7.0 and 4.4, however, is only a factor of 10, compared to an expected factor of 100–1000 due to base-catalyzed HX. Between pH 4.4 and 1.5, HX lifetimes have the same magnitude, while an ~1000-fold decrease is expected due to acid-catalyzed exchange. The stability of GCN4p based on urea denaturation experiments decreases by ~2 kcal/mol of dimer between pH 7 and 2,[8] so that changes in stability cannot account for the discrepancy in the pH dependence of HX lifetimes. Rather, the invariance of HX lifetimes with pH points to exchange occurring in the EX1 regime, where it is independent of pH.[51,52] In the EX1 regime, which is promoted at pH extremes by acid or base catalysis, HX depends on the kinetic rates of fluctuation that produce “open” exchange susceptible states. By contrast in the EX2 regime, the hallmark of which is a pH dependence of HX rates, HX depends on the stability of the structure. The HX periodicity at pH 7.0 is therefore probably lost at acidic pH, because in the EX1 limit localized dynamic fluctuations dominate HX processes to an extent that obscures the effects of hydrogen-bond length variations.

Acidic pH Leads to Increased Flexibility for Side Chains in Ion Pairs.

We next examined backbone dynamics on the picosecond to nanosecond time scale at the three pH values used for structure determination using $^{1}H–^{15}N$ NOE cross-relaxation (Figure 7). The $^{1}H–^{15}N$ NOE values are close to the theoretical maximum of 0.8, showing that the α-helix monomers remain stably folded over the entire pH range. There is a slight decrease in the baseline mean value for the $^{1}H–^{15}N$ NOEs, from ~0.8 at pH 6.6 (Figure 7A) to ~0.7 at pH 1.5 (Figure 7C). This suggests a small increase in backbone flexibility between the two pH values that may be related to the precision of the pH 1.5 NMR (Figure 4D) structures being slightly lower than the precision of those determined at pH 6.6 (Figure 4B).

Because changes in backbone dynamics of GCN4p were minimal, we wanted to see if a decrease in pH might have a stronger effect on side-chain dynamics. To investigate side-chain dynamics, we measured ^{13}C rotating frame T_1 relaxation values ($T_{1\rho}$) for methylene groups in GCN4p. Wherever possible, the methylene carbons farthest from the backbone were selected, as indicated on the *x*-axis of Figure 8. The ^{13}C relaxation data are represented as $R_{1\rho}$ values, where $R_{1\rho} = 1/T_{1\rho}$. Data obtained at pH 6.6 and 1.5 are shown with gray and white bars, respectively. For most of the sites, the $R_{1\rho}$ values at pH 1.5 are smaller than at pH 6.6, indicating an overall increase in side-chain flexibility at lower pH (Figure 8). Particularly large differences occur for the sites denoted by the arrows, corresponding to four acidic and basic residues in the ion pairs of GCN4p: E11 (E11–K8), E20 (E20–K15′), E22 (both E22–R25 and E22–K27′), and R25 (E22–R25). The remaining acidic and basic residues could not be resolved in the NMR spectrum. The results suggest that there is an increase in side-chain flexibility at low pH, with the increase being especially large for residues in the ion pairs that are disrupted at acidic pH.

DISCUSSION

There has been considerable controversy regarding the role of charge–charge interactions in stabilizing coiled coil structures.[12,20] The sequences of coiled coils lend themselves to ion pair formation,[18,49] and numerous studies have found that ion pairs contribute to the stabilities of coiled coils.[10,20,53] The GCN4p structure 2ZTA,[14] the first X-ray structure of a coiled coil dimer, shows many of the ion pairs predicted from the amino acid sequence, but these are not conserved between the two chains in the dimer or in some of the other X-ray structures of GCN4p. Mutagenesis of the charged residues that participate in the ion pairs can lead to large stability losses; however, such substitutions can have multifarious effects, extending beyond a perturbation of the Coulombic energy between two charges.[8,1] NMR studies show that the pH titratable residues of GCN4p have only small shifts in pK_a values from random coil models, suggesting that the charging of these residues makes only small contributions to stability.[8,12,48] In at least one case, E20, the pK_a shift is more consistent with a residue being involved in a destabilizing repulsive interaction between like charges than in a stabilizing ion pair.[12] To better understand the roles of electrostatic interactions in stabilizing coiled coils, we determined a complete set of pK_a values for all pH titratable acidic and basic residues in GCN4p.[8] The shifts of the pK_a values determined by NMR from random coil models were used to calculate contributions to the stability of GCN4p from the titration of individual sites, and these contributions were compared to stability data from urea denaturation curves followed by CD (circular dichroism) over a range of pH values from 2 to 12. Both numerical integration of the differences in proton binding calculated from NMR-derived pK_a shifts between the native and denatured state and pK_a values calculated from the 2ZTA X-ray structure failed to match the experimental stability data at low pH.[8] The experimental value for the stability of GCN4p based on urea denaturation experiments decreases from 9 kcal/mol of dimer at pH 7 to 7 kcal/mol of dimer at pH 2.[8] The stability predicted at pH 2 from the 2ZTA X-ray structure of GCN4p (determined at pH 7) was ~5 kcal/mol of dimer, an underestimate of ~2 kcal/mol of dimer. By contrast, the stability at pH 2 predicted from the pK_a differences between the native protein and random coil values was ~8.5 kcal/mol of dimer,[8] an overestimate of 1.5 kcal/mol of dimer.[8] As discussed below, neither the assumption that the structure of GCN4p is invariant between neutral and acidic pH nor the assumption that the GCN4p coiled coil unfolds in a strict two-state transition is likely to be correct.

The NMR structures determined in this work show that while the coiled coil motif is conserved, there are changes in the structure and dynamics of GCN4p at low pH. These include (i) a partial unwinding of the coiled coil superhelix, (ii) a small increase in the separation between the α-helix monomers, (iii) a loosening of the knobs-into-holes packing near the chain termini of the coiled coil, and (iv) an increase in side-chain dynamics, particularly for residues that participate in ion pairs at neutral pH. The increase in flexibility of titratable residues as ion pairs become broken could be due to the weakening of interactions between charged groups on the protein or changes in the interactions between the charged groups and solvent. The intermolecular E20–K15′ and E22–K27′ ion pairs bring together residues in nonequivalent sequence positions across the dimer interface, which favors supercoiling of the structure. Disruption of the intermolecular ion pairs is thus

likely to account for the partial unwinding of the coiled coil superhelix observed in the NMR structures at low pH. In as much as interchain charge interactions are favored between heptad e and g positions, at a separation of five residues, ion pairs could play a general role in determining supercoiling in addition to the packing of hydrophobic residues.

The changes in structure and dynamics accompanying acidification suggest that the 2ZTA X-ray structure of GCN4p determined at neutral pH is not an appropriate model for the behavior of the coiled coil at extremes of pH. The difference between neutral and acidic pH is not just a turning off of electrostatic interactions. Structural rearrangements in the protein, and possibly between the protein and solvent, accompany the loss of ion pairs at acidic pH. These differences, for example, a favorable entropic contribution from the increase in side-chain dynamics at acid pH, may be why the use of the neutral-pH 2ZTA X-ray structure underestimates the stability of the coiled coil at low pH.[8]

By contrast, integration of the pK_a shifts between the GCN4p coiled coil and random coil model compounds overestimates the contributions of ion pairs to unfolding stability at low pH. In spite of the structural evidence supporting the intermolecular E20–K15′ and E22–K27′ ion pairs at neutral pH, the acidic residues involved, E20 and E22, have pK_a values of 4.4 and 4.2, respectively, compared to the random coil value for glutamate of 4.25.[8] Note that E22 is also involved in the intramolecular E22–R25 ion pair (Table 2). It is possible to calculate the change in stability of a protein from the protonation of a residue, using a thermodynamic linkage analysis that considers the shift in pK_a of the native state compared to that of the denatured state: $\Delta\Delta G_{titr} = \Delta G_U - \Delta G_{UH} = -2.303RT(pK_a^U - pK_a^F)$.[12,54] Using this analysis, the contribution from protonation of E22 at low pH is close to zero while that for E20 is positive (~0.4 kcal/mol of dimer depending on the random coil model), indicating an unfavorable contribution from the charged state of the glutamate, possibly due to a repulsive interaction between like charges.[8,12] At the same time, the R25A mutation that disrupts the E22–R25 ion pair causes a large decrease in the stability of GNC4p[10] and of the coiled coil trigger site.[55] Of the acidic residues in GCN4p ion pairs (Table 2), only the charged state of E11 stabilizes the coiled coil by 1 kcal/mol of dimer, based on the pK_a shift between its native (pK_a = 4.05) and unfolded (pK_a = 4.40) state.[8] There thus appears to be an apparent discrepancy between the changes in the NMR structures at different pH values, and the relatively small favorable and unfavorable contributions to the stability of the coiled coil predicted by the thermodynamic linkage analysis of pK_a values.[8,12,54] The first reason for this disagreement is that the thermodynamic linkage analysis assumes pairwise electrostatic interactions (e.g., ion pairs), and that contributions can be separated from other effects, like changes in structure or solvation. Electrostatic interactions in GCN4p may in fact be more like a diffuse network of couplings between multiple charges. For example, E22 participates in an intramolecular interaction with R25 and an intermolecular interaction with K27′ (Table 2) and may be affected by a repulsive interactions with E22′ from the other monomer.[12] A second assumption of the thermodynamic linkage analysis is that the molecule is in a two-state equilibrium between folded and unfolded states.[54] There is in fact evidence of an “X form” of GCN4p, which corresponds to a monomer with partially folded α-helical structure at acidic pH.[13] The X form is promoted at the expense of the coiled coil dimer at acidic pH and low peptide concentrations. In the study presented here, the X form was largely suppressed by working with 1.5 mM GCN4p, a concentration 100-fold higher

than the GCN4p concentration of 15 μM at which the X form dominates.[13] Nevertheless at pH 1.5, the most acidic condition studied, we observe a trace amount of the X form in ^{1}H–^{15}N HSQC spectra (Figure 1C) with an X form/coiled coil cross-peak volume ratio of ~0.15. Indeed, the changes in the GCN4p NMR structures described in this work, which point to a weakening of the dimerization interface at low pH, may provide a mechanism for the formation of the monomeric X form. Additional evidence that GCN4p can sustain α-helical structures in monomeric forms includes the p16–31 fragment corresponding to the coiled coil "trigger site", which has an α-helical content of ~50% at neutral pH and a temperature of 5 °C.[55] While there are differences in the CD spectra of regular and coiled coil α-helices that arise from the superhelix twist, the effects are rather subtle.[56] It would certainly not be possible to distinguish between an α-helical monomer (e.g., the X form) from a coiled coil dimer using CD ellipticity at a single wavelength such as 222 nm, the method used to measure the pH dependence of GCN4p stability to urea unfolding.[8] Thus, the assumption of a two-state unfolding could interfere with stability measurements, because when the coiled coil breaks into α-helical monomers these will still contain residual α-helix structure that contributes to ellipticity at 222 nm. Similarly in a multistate model in which the coiled coil dimer can dissociate to a monomer with residual α-helical structure, the pK_a values of the latter may be inaccurately described by the random coil reference state, leading to errors in the predicted unfolding stability at extremes of pH.

The motivation for this study was to see how the GCN4p structure responds to changes in pH that disrupt ion pairs. To this end, we determined NMR structures at three pH values where the ion pairs are fully formed, half-populated, and fully broken. The predominant changes in the structures with a decrease in pH include an unwinding of the coiled coil and an increase in the separation of oppositely charged residues that participate in ion pairs. When coupled with dynamics data that show the flexibility of the α-helix monomers is conserved but that there are increases in the extent of motion for side chains that participate in the dimerization interface, the observations shed new light on the roles of ion pairs in maintaining the coiled coil structure. The possibility of following molecular structure as a function of solution conditions is an inherent advantage of NMR and represents a relatively unexplored frontier. There is clearly room for methodological improvements, including increasing the efficiency of structure determination, for example, using only a subset of data. The potential for NMR to determine structures of molecules visiting multiple conformational states promises the reward of a richer understanding of processes important in all aspects of molecular biology, including protein folding, binding, and function.

Supplementary Material

Refer to Web version on PubMed Central for supplementary material.

Acknowledgments

Funding

This work was supported by a National Science Foundation Graduate Research Fellowship to A.R.K. and a UConn Summer Undergraduate Research Fellowship to M.R.B.

ABBREVIATIONS

CD	circular dichroism
D_2O	deuterium oxide
FID	free induction decay
H-bond	hydrogen bond
HSQC	heteronuclear single-quantum correlation
HX	hydrogen exchange
NMR	nuclear magnetic resonance
NOE	nuclear Overhauser enhancement
NOESY	nuclear Overhauser enhancement spectroscopy
RMSD	root-mean-square deviation
$T_{1\rho}$	T_1 relaxation in the rotating frame

REFERENCES

(1). Wuthrich K (2003) NMR studies of structure and function of biological macromolecules (Nobel lecture). Angew. Chem., Int. Ed. 42, 3340–3363.

(2). Clore GM, and Gronenborn AM (1991) Two-, three-, and four-dimensional NMR methods for obtaining larger and more precise three-dimensional structures of proteins in solution. Annu. Rev. Biophys. Biophys. Chem 20, 29–63. [PubMed: 1651086]

(3). Tugarinov V, Hwang PM, and Kay LE (2004) Nuclear magnetic resonance spectroscopy of high-molecular-weight proteins. Annu. Rev. Biochem 73, 107–146. [PubMed: 15189138]

(4). Davies TG, and Tickle IJ (2011) Fragment screening using X-ray crystallography. Top. Curr. Chem 317, 33–59.

(5). Perutz MF (1978) Hemoglobin structure and respiratory transport. Sci. Am 239, 92–125.

(6). Chimenti MS, Khangulov VS, Robinson AC, Heroux A, Majumdar A, Schlessman JL, and Garcia-Moreno B (2012) Structural reorganization triggered by charging of Lys residues in the hydrophobic interior of a protein. Structure 20, 1071–1085. [PubMed: 22632835]

(7). Karp DA, Gittis AG, Stahley MR, Fitch CA, Stites WE, and Garcia-Moreno E B (2007) High apparent dielectric constant inside a protein reflects structural reorganization coupled to the ionization of an internal Asp. Biophys. J 92, 2041–2053. [PubMed: 17172297]

(8). Matousek WM, Ciani B, Fitch CA, Garcia-Moreno E B, Kammerer RA, and Alexandrescu AT (2007) Electrostatic contributions to the stability of the GCN4 leucine zipper structure. J. Mol. Biol 374, 206–219. [PubMed: 17920624]

(9). Steinmetz MO, Jelesarov I, Matousek WM, Honnappa S, Jahnke W, Missimer JH, Frank S, Alexandrescu AT, and Kammerer RA (2007) Molecular basis of coiled-coil formation. Proc. Natl. Acad. Sci. U. S. A 104, 7062–7067. [PubMed: 17438295]

(10). Kammerer RA, Jaravine VA, Frank S, Schulthess T, Landwehr R, Lustig A, Garcia-Echeverria C, Alexandrescu AT, Engel J, and Steinmetz MO (2001) An intrahelical salt bridge within the trigger site stabilizes the GCN4 leucine zipper. J. Biol. Chem 276, 13685–13688. [PubMed: 11134036]

(11). Goodman EM, and Kim PS (1991) Periodicity of amide proton exchange rates in a coiled-coil leucine zipper peptide. Biochemistry 30, 11615–11620. [PubMed: 1661141]

(12). Lumb KJ, and Kim PS (1995) Measurement of interhelical electrostatic interactions in the GCN4 leucine zipper. Science 268, 436–439. [PubMed: 7716550]

(13). Nikolaev Y, and Pervushin K (2007) NMR spin state exchange spectroscopy reveals equilibrium of two distinct conformations of leucine zipper GCN4 in solution. J. Am. Chem. Soc 129, 6461–6469. [PubMed: 17469817]

(14). O'Shea EK, Klemm JD, Kim PS, and Alber T (1991) Xray structure of the GCN4 leucine zipper, a two-stranded, parallel coiled coil. Science 254, 539–544. [PubMed: 1948029]

(15). Zitzewitz JA, Bilsel O, Luo J, Jones BE, and Matthews CR (1995) Probing the folding mechanism of a leucine zipper peptide by stopped-flow circular dichroism spectroscopy. Biochemistry 34, 12812–12819. [PubMed: 7548036]

(16). O'Donoghue SI, Junius FK, and King GF (1993) Determination of the structure of symmetric coiled-coil proteins from NMR data: application of the leucine zipper proteins Jun and GCN4. Protein Eng., Des. Sel 6, 557–564.

(17). Saudek V, Pastore A, Morelli MA, Frank R, Gausepohl H, and Gibson T (1991) The solution structure of a leucine-zipper motif peptide. Protein Eng., Des. Sel 4, 519–529.

(18). Burkhard P, Kammerer RA, Steinmetz MO, Bourenkov GP, and Aebi U (2000) The coiled-coil trigger site of the rod domain of cortexillin I unveils a distinct network of interhelical and intrahelical salt bridges. Structure 8, 223–230. [PubMed: 10745004]

(19). Lupas AN, and Gruber M (2005) The structure of alphahelical coiled coils. Adv. Protein Chem 70, 37–78. [PubMed: 15837513]

(20). Lavigne P, Kay CM, Sonnichsen FD, Hodges RS, Lumb KJ, and Kim PS (1996) Interhelical salt bridges, coiled-coil stability, and specificity of dimerization. Science 271, 1136–1138. [PubMed: 8599093]

(21). Berisio R, Lamzin VS, Sica F, Wilson KS, Zagari A, and Mazzarella L (1999) Protein titration in the crystal state. J. Mol. Biol 292, 845–854. [PubMed: 10525410]

(22). Croke RL, Sallum CO, Watson E, Watt ED, and Alexandrescu AT (2008) Hydrogen exchange of monomeric alphasynuclein shows unfolded structure persists at physiological temperature and is independent of molecular crowding in Escherichia coli. Protein Sci. 17, 1434–1445. [PubMed: 18493022]

(23). Grigoryan G, and Degrado WF (2011) Probing designability via a generalized model of helical bundle geometry. J. Mol. Biol 405, 1079–1100. [PubMed: 20932976]

(24). Walshaw J, and Woolfson DN (2003) Extended knobs-intoholes packing in classical and complex coiled-coil assemblies. J. Struct. Biol 144, 349–361. [PubMed: 14643203]

(25). Kammerer RA, Schulthess T, Landwehr R, Lustig A, Engel J, Aebi U, and Steinmetz MO (1998) An autonomous folding unit mediates the assembly of two-stranded coiled coils. Proc. Natl. Acad. Sci. U. S. A 95, 13419–13424. [PubMed: 9811815]

(26). Kammerer RA, Schulthess T, Landwehr R, Lustig A, Fischer D, and Engel J (1998) Tenascin-C hexabrachion assembly is a sequential two-step process initiated by coiled-coil alpha-helices. J. Biol. Chem 273, 10602–10608. [PubMed: 9553121]

(27). Wiltscheck R, Kammerer RA, Dames SA, Schulthess T, Blommers MJ, Engel J, and Alexandrescu AT (1997) Heteronuclear NMR assignments and secondary structure of the coiled coil trimerization domain from cartilage matrix protein in oxidized and reduced forms. Protein Sci. 6, 1734–1745. [PubMed: 9260286]

(28). Vranken WF, Boucher W, Stevens TJ, Fogh RH, Pajon A, Llinas M, Ulrich EL, Markley JL, Ionides J, and Laue ED (2005) The CCPN data model for NMR spectroscopy: development of a software pipeline. Proteins: Struct., Funct., Genet 59, 687–696. [PubMed: 15815974]

(29). Wishart DS, Bigam CG, Yao J, Abildgaard F, Dyson HJ, Oldfield E, Markley JL, and Sykes BD (1995) 1H, 13C and 15N chemical shift referencing in biomolecular NMR. J. Biomol. NMR 6, 135–140. [PubMed: 8589602]

(30). Wishart DS, Bigam CG, Holm A, Hodges RS, and Sykes BD (1995) 1H, 13C and 15N random coil NMR chemical shifts of the common amino acids. I. Investigations of nearest-neighbor effects. J. Biomol. NMR 5, 67–81. [PubMed: 7881273]

(31). Dames SA, Kammerer RA, Wiltscheck R, Engel J, and Alexandrescu AT (1998) NMR structure of a parallel homotrimeric coiled coil. Nat. Struct. Mol. Biol 5, 687–691.

(32). Shen Y, and Bax A (2015) Protein structural information derived from NMR chemical shift with the neural network program TALOS-N. Methods Mol. Biol 1260, 17–32. [PubMed: 25502373]

(33). Schwieters CD, Kuszewski JJ, Tjandra N, and Marius Clore G (2003) The Xplor-NIH NMR molecular structure determination package. J. Magn. Reson 160, 65–73. [PubMed: 12565051]

(34). Rieping W, Habeck M, Bardiaux B, Bernard A, Malliavin TE, and Nilges M (2007) ARIA2: automated NOE assignment and data integration in NMR structure calculation. Bioinformatics 23, 381–382. [PubMed: 17121777]

(35). The PyMOL Molecular Graphics System, version 1.8, Schrödinger, LLC, Portland, OR.

(36). Newcomer RL, Fraser LC, Teschke CM, and Alexandrescu AT (2015) Mechanism of Protein Denaturation: Partial Unfolding of the P22 Coat Protein I-Domain by Urea Binding. Biophys. J 109, 2666–2677. [PubMed: 26682823]

(37). Alexandrescu AT, and Shortle D (1994) Backbone dynamics of a highly disordered 131 residue fragment of staphylococcal nuclease. J. Mol. Biol 242, 527–546. [PubMed: 7932708]

(38). Greenfield NJ, Huang YJ, Palm T, Swapna GV, Monleon D, Montelione GT, and Hitchcock-DeGregori SE (2001) Solution NMR structure and folding dynamics of the N terminus of a rat non-muscle alpha-tropomyosin in an engineered chimeric protein. J. Mol. Biol 312, 833–847. [PubMed: 11575936]

(39). Pauling L, and Corey RB (1953) Compound helical configurations of polypeptide chains: structure of proteins of the alpha-keratin type. Nature 171, 59–61. [PubMed: 13025480]

(40). Blundell T, Barlow D, Borkakoti N, and Thornton J (1983) Solvent-induced distortions and the curvature of alphα-helices. Nature 306, 281–283. [PubMed: 6646210]

(41). Hori Y, Demura M, Iwadate M, Ulrich AS, Niidome T, Aoyagi H, and Asakura T (2001) Interaction of mastoparan with membranes studied by 1H-NMR spectroscopy in detergent micelles and by solid-state 2H-NMR and 15N-NMR spectroscopy in oriented lipid bilayers. Eur. J. Biochem 268, 302–309. [PubMed: 11168364]

(42). Patil SM, Xu S, Sheftic SR, and Alexandrescu AT (2009) Dynamic alphα-helix structure of micelle-bound human amylin. J. Biol. Chem 284, 11982–11991. [PubMed: 19244249]

(43). Rao JN, Kim YE, Park LS, and Ulmer TS (2009) Effect of pseudorepeat rearrangement on alpha-synuclein misfolding, vesicle binding, and micelle binding. J. Mol. Biol 390, 516–529. [PubMed: 19481090]

(44). Nilges M (1993) A calculation strategy for the structure determination of symmetric dimers by 1H NMR. Proteins: Struct., Funct., Genet 17, 297–309. [PubMed: 8272427]

(45). Lee W, Revington MJ, Arrowsmith C, and Kay LE (1994) A pulsed field gradient isotope-filtered 3D 13C HMQC-NOESY experiment for extracting intermolecular NOE contacts in molecular complexes. FEBS Lett. 350, 87–90. [PubMed: 8062930]

(46). Wagner G, Hyberts SG, and Havel TF (1992) NMR structure determination in solution: a critique and comparison with Xray crystallography. Annu. Rev. Biophys. Biomol. Struct 21, 167–198. [PubMed: 1525468]

(47). Crick FH (1953) The fourier transform of a coiled coil. Acta Crystallogr. 6, 685–689.

(48). Dames SA, Kammerer RA, Moskau D, Engel J, and Alexandrescu AT (1999) Contributions of the ionization states of acidic residues to the stability of the coiled coil domain of matrilin-1. FEBS Lett. 446, 75–80. [PubMed: 10100618]

(49). Mason JM, and Arndt KM (2004) Coiled coil domains: stability, specificity, and biological implications. ChemBioChem 5, 170–176. [PubMed: 14760737]

(50). Bai Y, Milne JS, Mayne L, and Englander SW (1993) Primary structure effects on peptide group hydrogen exchange. Proteins: Struct., Funct., Genet 17, 75–86. [PubMed: 8234246]

(51). Bai Y, Milne JS, Mayne L, and Englander SW (1994) Protein stability parameters measured by hydrogen exchange. Proteins: Struct., Funct., Genet 20, 4–14. [PubMed: 7824522]

(52). Clarke J, and Fersht AR (1996) An evaluation of the use of hydrogen exchange at equilibrium to probe intermediates on the protein folding pathway. Folding Des. 1, 243–254.

(53). Zhou NE, Kay CM, and Hodges RS (1994) The net energetic contribution of interhelical electrostatic attractions to coiledcoil stability. Protein Eng., Des. Sel 7, 1365–1372.

(54). Sheftic SR, Croke RL, LaRochelle JR, and Alexandrescu AT (2009) Electrostatic contributions to the stabilities of native proteins and amyloid complexes. Methods Enzymol. 466, 233–258. [PubMed: 21609864]

(55). Steinmetz MO, Jelesarov I, Matousek WM, Honnappa S, Jahnke W, Missimer JH, Frank S, Alexandrescu AT, and Kammerer RA (2007) Molecular basis of coiled-coil formation. Proc. Natl. Acad. Sci. U. S. A 104, 7062–7067. [PubMed: 17438295]

(56). Cooper TM, and Woody RW (1990) The effect of conformation on the CD of interacting helices: a theoretical study of tropomyosin. Biopolymers 30, 657–676. [PubMed: 2275971]

(57). Nabuurs SB, Spronk CA, Krieger E, Maassen H, Vriend G, and Vuister GW (2003) Quantitative evaluation of experimental NMR restraints. J. Am. Chem. Soc 125, 12026–12034. [PubMed: 14505424]

(58). Bhattacharya A, Tejero R, and Montelione GT (2007) Evaluating protein structures determined by structural genomics consortia. Proteins: Struct., Funct., Genet 66, 778–795. [PubMed: 17186527]

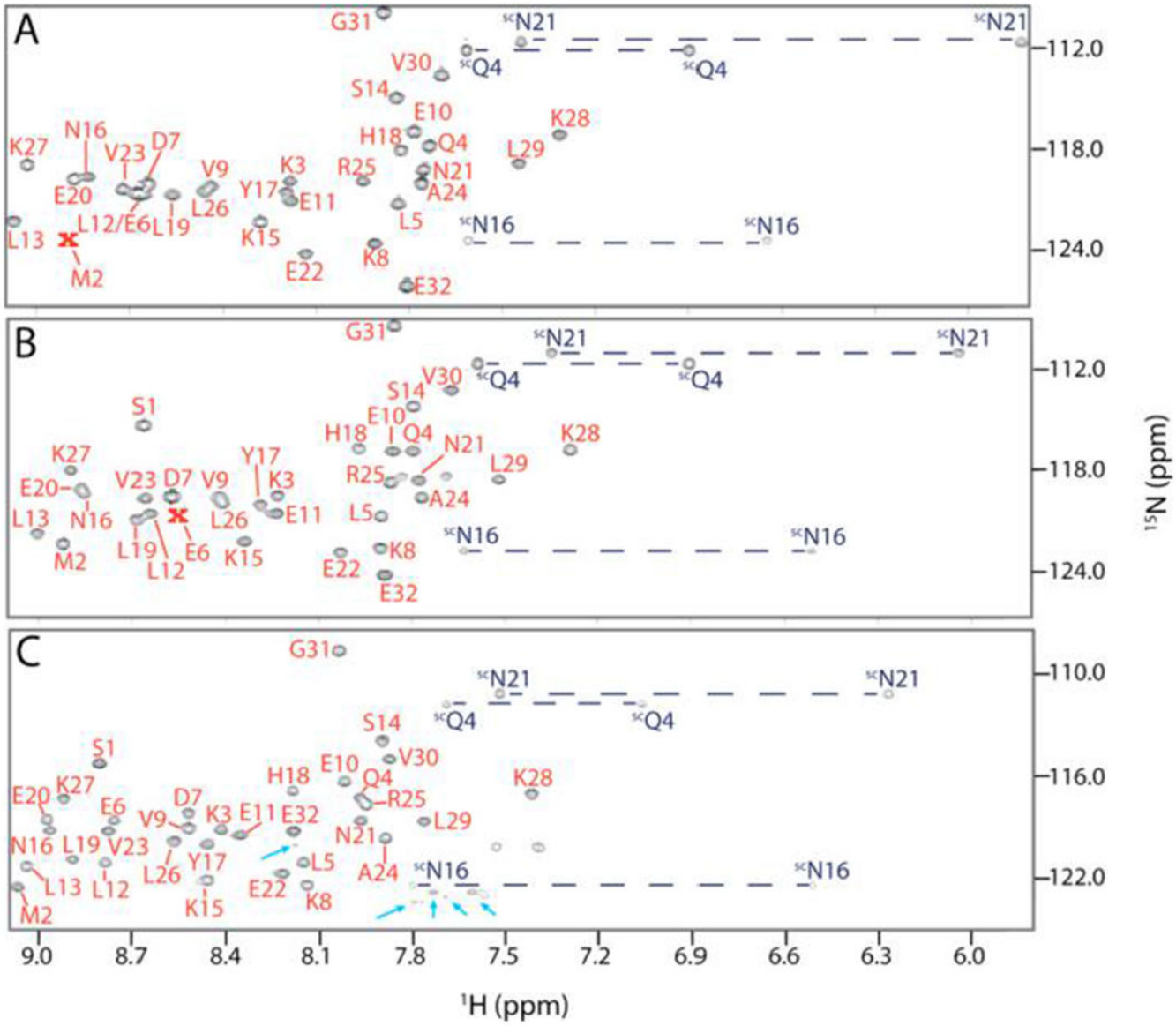

Figure 1.

^{1}H–^{15}N HSQC spectra of GCN4p at pH (A) 6.6, (B) 4.4, and (C) 1.5. Peaks below the contour level shown are marked with the symbol "X". Cross-peaks from Asn and Gln side-chain amide protons are connected by dashed horizontal lines, labeled in black type, and marked with the superscript "sc". The side-chain amide protons of N16 are folded in the ^{15}N dimension. The residue numbering scheme used in this and subsequent figures is the same as that of the GNC4p X-ray structure (PDB entry 2ZTA). Blue arrows in panel C indicate cross-peaks from trace amounts of the X form, which is stabilized at low pH.

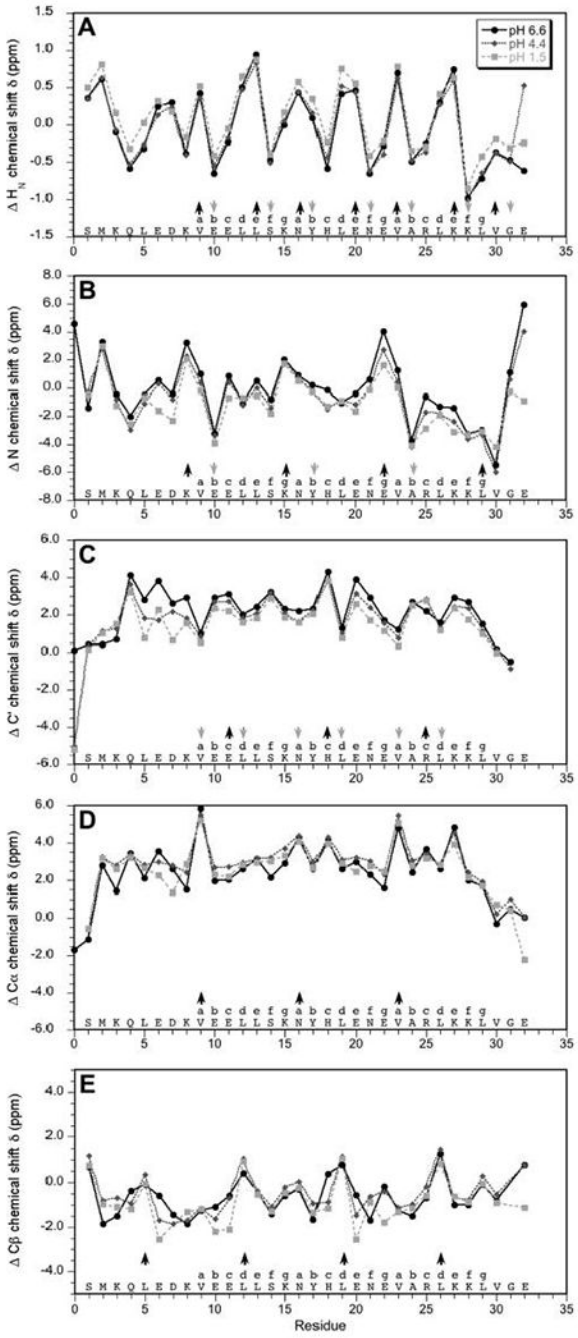

Figure 2.

Chemical shift differences from random coil values. (A) HN, (B) N, (C) C′, (D) Cα, and (E) Cβ nuclei. Sequence and heptad repeat positions are given in each panel. Arrows denote periodicity in chemical shift values with respect to heptad repeat positions, with black and gray arrows indicating large and small chemical shift deviations, respectively.

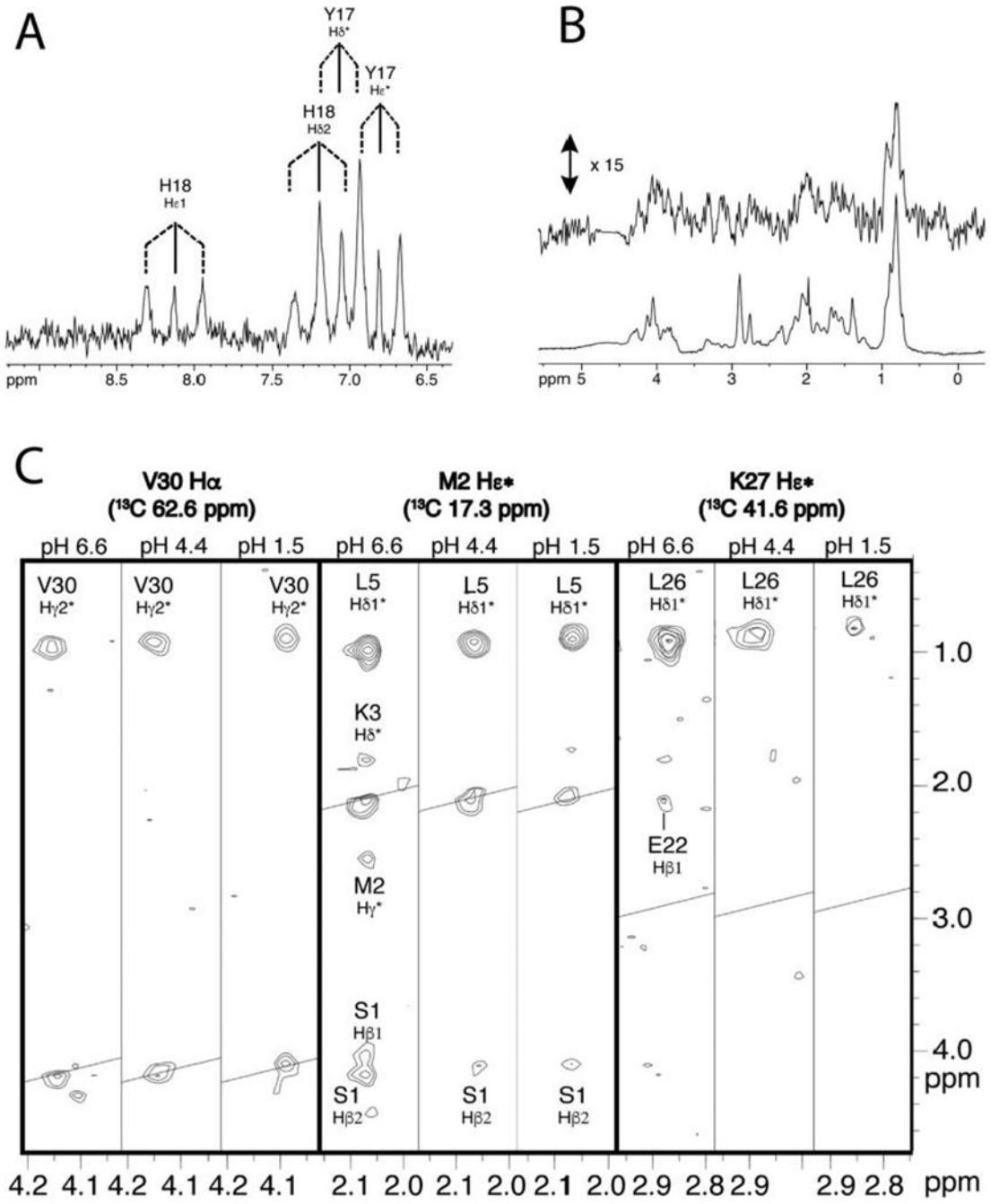

Figure 3.

^{13}C isotope-filtered NOESY experiments with GCN4p. (A) Aromatic region from a 1D ^{3}H NMR spectrum of the ^{12}C/^{13}C mixed dimer sample of GCN4p at pH 6.6, demonstrating the mixture of the ^{12}C and ^{13}C chains. (B) Illustration of the efficiency of NOE transfer between ^{12}C and ^{13}C chains. The bottom trace shows the ^{13}C-edited 1D NMR spectrum of the mixed ^{12}C/^{13}C mixed dimer GCN4p sample at pH 6.6 (obtained by averaging 16 transients in 0.25 min and processed with a line broadening of 2 Hz). The top trace is the first FID of the corresponding 3D ^{13}C-F1-filtered, ^{13}C-F3-edited NOESY-HSQC spectrum (obtained by

averaging 256 transients in 4 min, processed with a line broadening of 10 Hz, and shown at 15 times the vertical scale). Because of the poor sensitivity of NOE transfer, the corresponding 3D ^{13}C-F1-filtered, ^{13}C-F3-edited NOESY-HSQC experiment was performed for 6.5 days (corresponding to averaging of ~360000 transients). (C) Comparisons of representative strips from ^{13}C planes of the 3D ^{13}C-filtered NOESY spectra recorded at each of the three pH values. The diagonal is indicated in each strip.

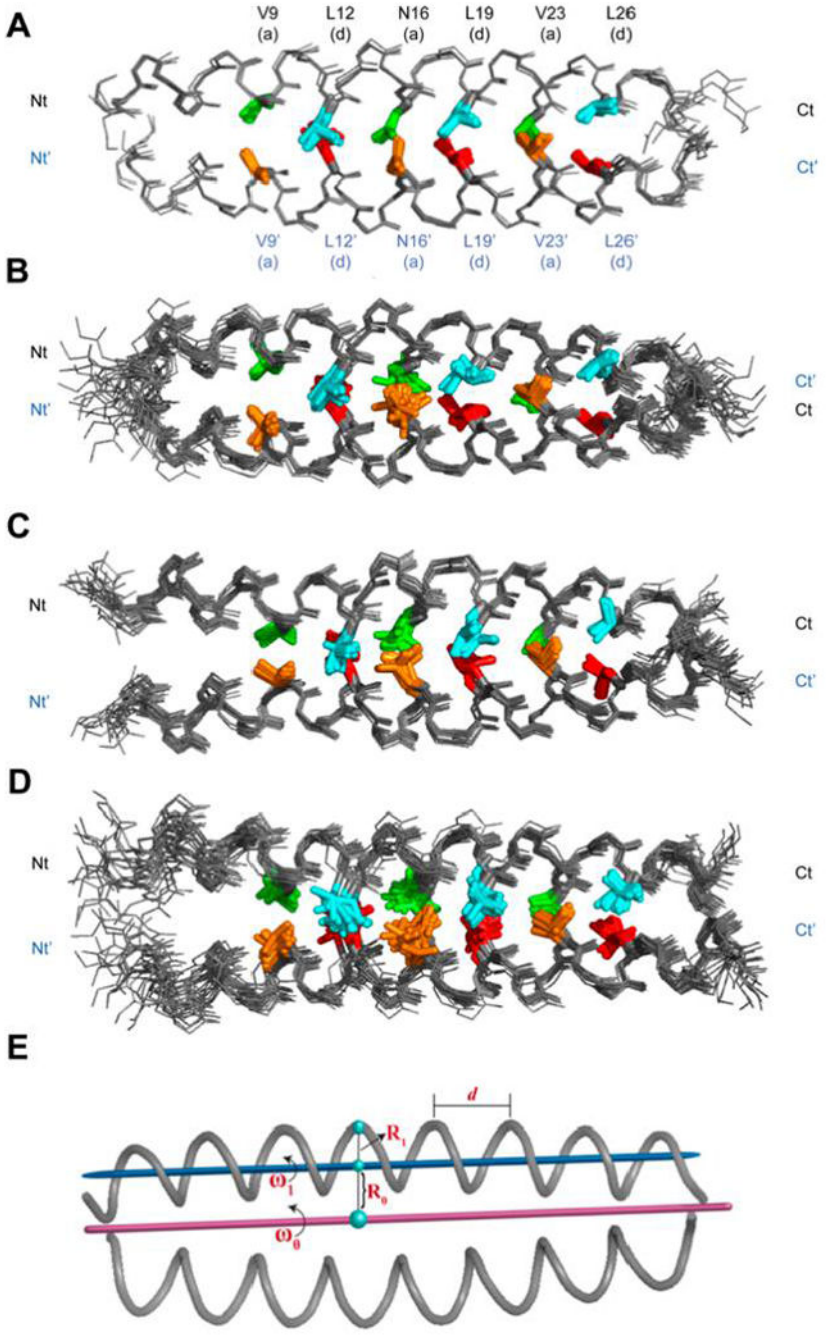

Figure 4.

Backbone structures of GCN4p. (A) Set of six X-ray structures determined between pH 8.5 and 6.0 (PDB entries 2ZTA, 1ZII, 1ZIK, 1ZIL, 2AHP, and 4TL1). NMR ensemble of the best 20 structures at (B) pH 6.6, (C) pH 4.4, and (D) pH 1.5. Backbone atoms (C′, N, Cα, and O) are colored gray. Side-chain atoms of the 2-fold symmetry-related monomers are labeled according to their sequence and heptad repeat positions (**a**, green and orange; **d**, cyan and red). (E) Ribbon diagram of the 2ZTA X-ray structure illustrating the Crick parameters used for analysis of the coiled coil structures (see Table 2 and the main text).

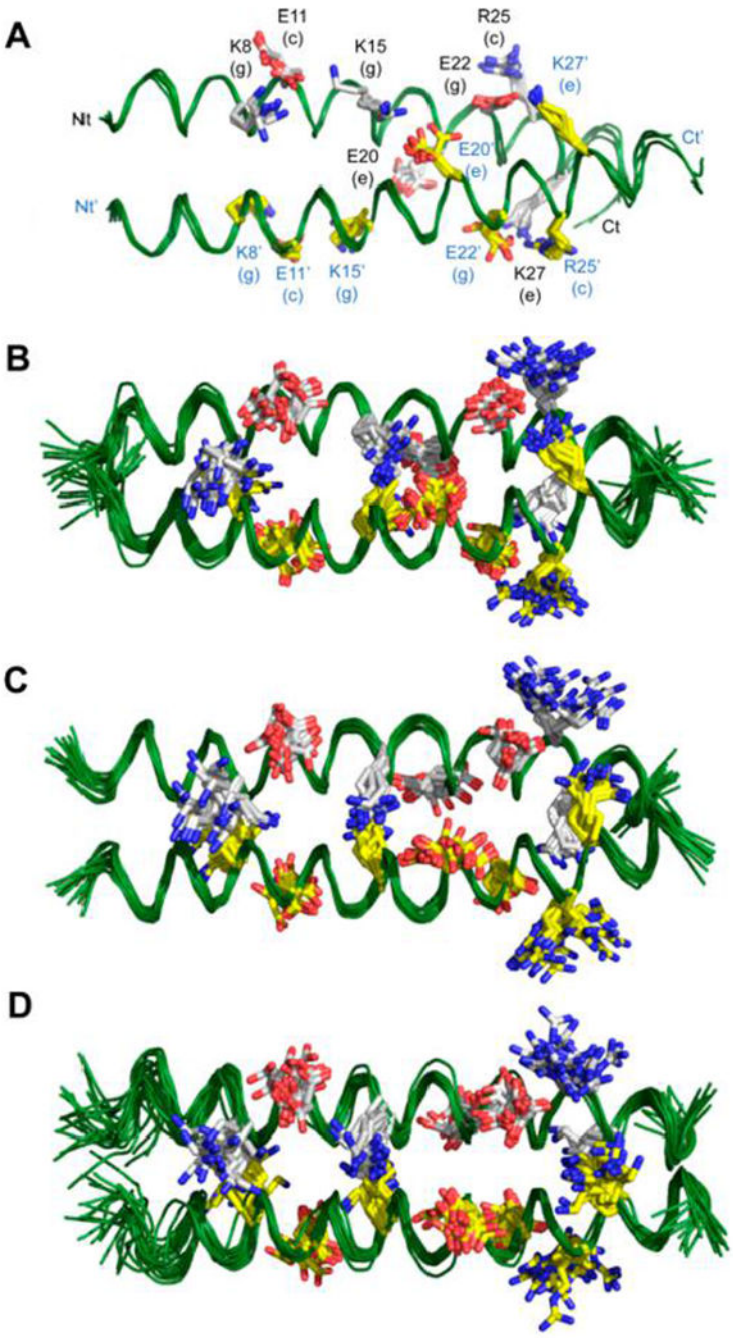

Figure 5.

Effects of pH on the precision of side-chain conformations for acidic and basic residues that have the potential to form ion pairs (see Table 2). (A) Reference set of six X-ray structures determined between pH 8.5 and 6.0. Ensembles of the 20 lowest-energy NMR structures at (B) pH 6.6, (C) pH 4.4, and (D) pH 1.5. Note that the pH-dependent increase in surface side-chain structure heterogeneity is larger than that for the buried hydrophobic residues in **a** and **d** heptad repeat positions (Figure 4).

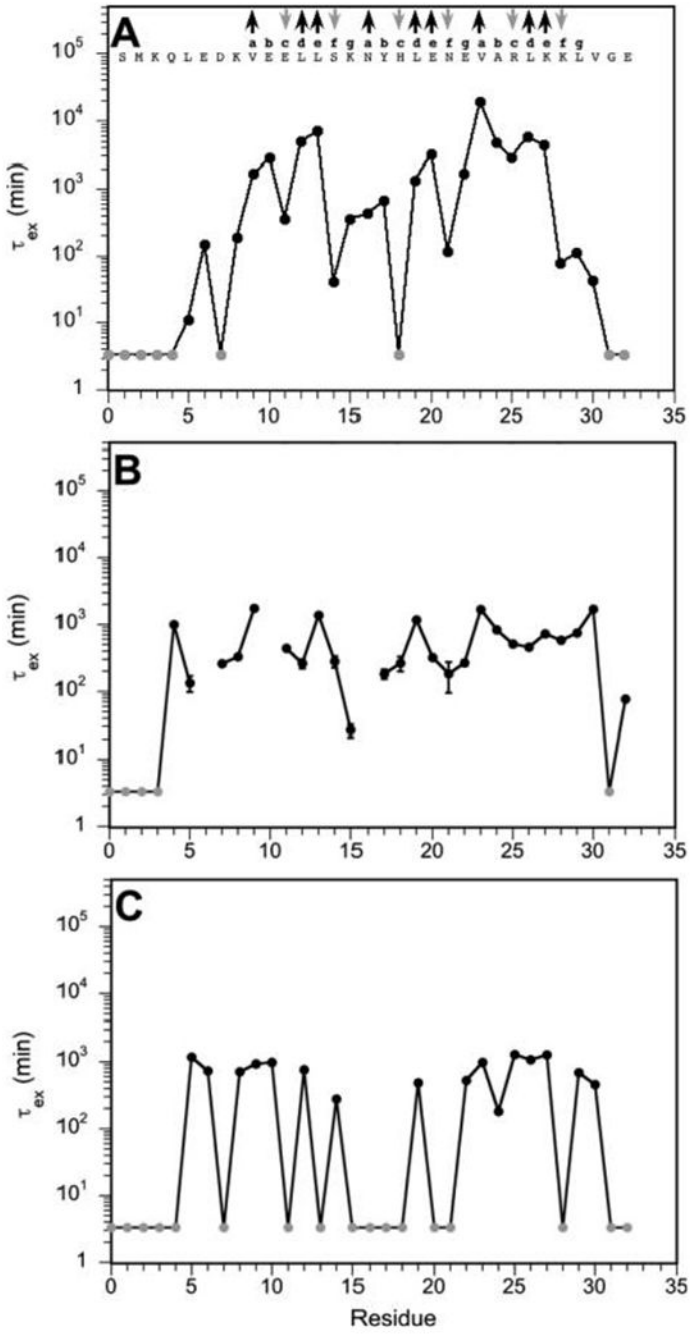

Figure 6.

Effects of pH on hydrogen exchange lifetimes: (A) pH 7.0, (B) pH 4.4, and (C) pH 1.5. The data at pH 7.0 where taken from a previously published paper[11] and are shown for comparison with the new results at pH 4.4 and 1.5 from this work. Experiments at pH 7 were performed at 6 °C, compared to 10 °C at pH 4.4 and 1.5. The periodicity in hydrogen exchange at pH 7 noted by Goodman and Kim[11] (A) is no longer observed at acidic pH values (B and C). Note the logarithmic scale for the *y*-axis. Gray data points indicate amide

protons that exchange too fast to measure. Gaps correspond to sites that could not be analyzed because of overlap in the spectrum.

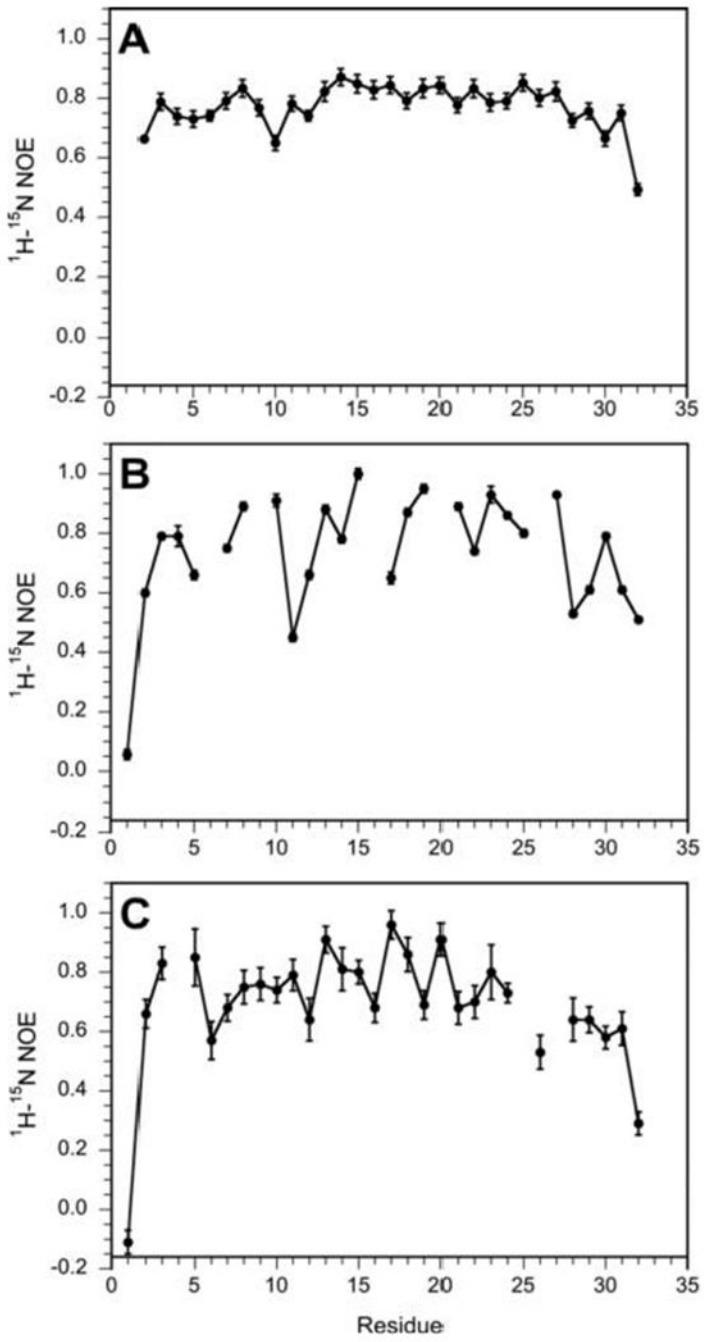

Figure 7.

Backbone dynamics investigated by ^{1}H–^{15}N NOEs at (A) pH 6.6, (B) pH 4.4, and (C) pH 1.5. All measurements were taken at 600 MHz and 25 °C.

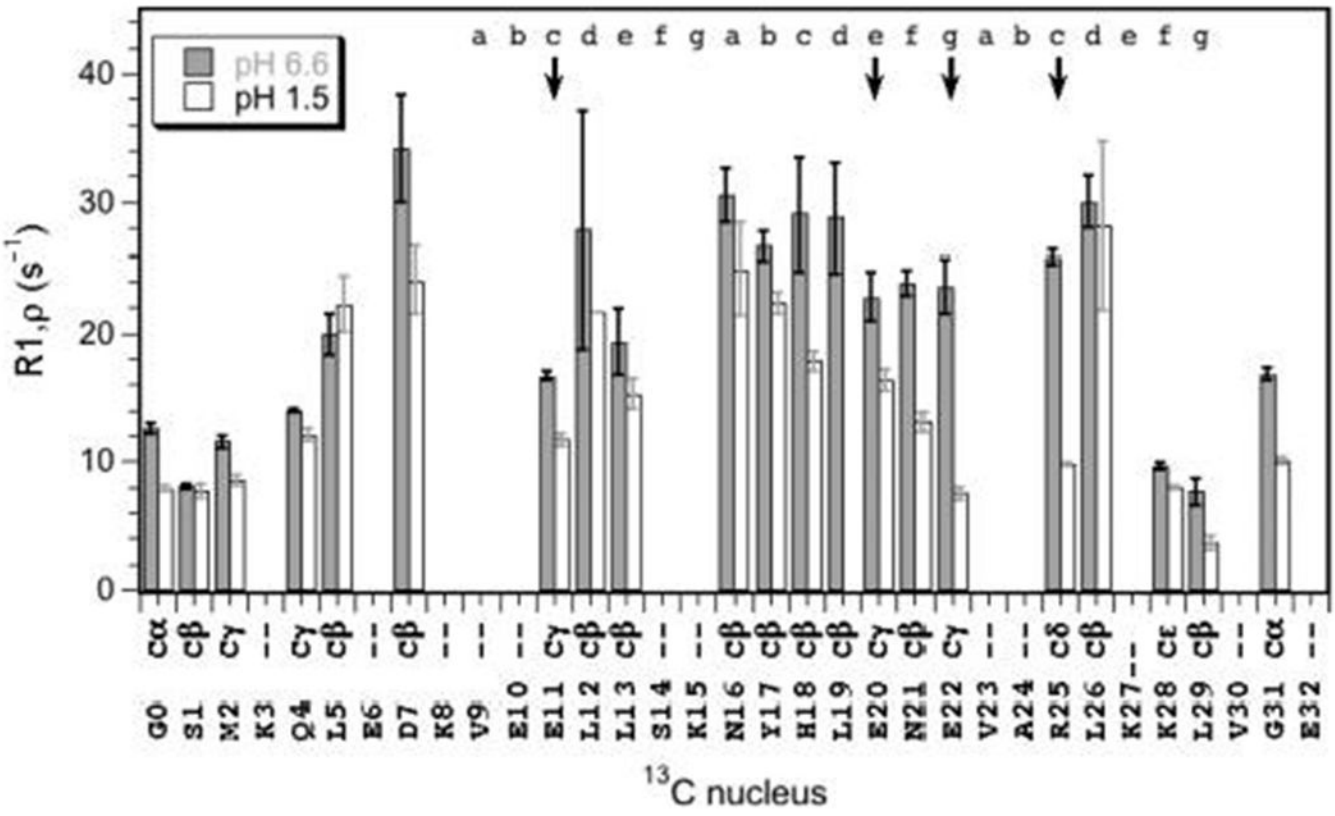

Figure 8.

Effects of pH on side-chain dynamics probed with ^{13}C $R_{1\rho}$ measurements of methylene carbons. All experiments were performed on a 600 MHz spectrometer at 25 °C. The relaxation rate, $R_{1\rho}$, is the inverse of the time constant for T_1 relaxation in the rotating frame ($R_{1\rho} = 1/T_{1\rho}$). Thus, sites with small $R_{1\rho}$ values (e.g., at the chain termini) have increased dynamics. The ^{13}C nuclei probed for each residue are identified on the *x*-axis of the plot, and the residue heptad repeat position is indicated at the top of the figure. Gray and white columns denote data obtained at pH 6.6 and 1.5, respectively. For L19, we could measure $R_{1\rho}$ only at pH 6.6. Arrows indicate acidic and basic residues that have a potential to form ion pairs and were resolved in NMR spectra. These sites show a large decrease in $R_{1\rho}$ from pH 6.6 to 1.5, indicating a large increase in side-chain dynamics at acidic pH.

Biochemistry. Author manuscript; available in PMC 2019 January 31.

Table 1.

Statistics for the 20 Lowest-Energy NMR Structures of GCN4p at Different pH Values

	pH 6.6	pH 4.4	pH 1.5
Experimental Restraints			
total no. of NMR restraints[a]	862	650	702
no. of distance restraints (total)	736	512	574
intraresidue NOEs	272	152	220
sequential NOEs[b]	150	116	150
medium-range NOEs ($\|i-j\| \leq 4$)[b]	154	96	102
long-range NOEs ($\|i-j\| > 4$)[b]	0	2	0
intrachain	576	366	472
interchain	108	94	70
hydrogen bonds (H-bond × 2)[c]	52	52	32
total no. of dihedral restraints	126	138	128
backbone (ϕ and ψ)	116	116	110
side chain (χ_1)	10	22	18
Residual Restraint Violations[d]			
NOE (Å)	0.042 ± 0.001	0.045 ± 0.001	0.043 ± 0.007
dihedral (deg)	0.18 ± 0.03	0.10 ± 0.02	0.05 ± 0.03
RMSD from Ideal Geometry			
bonds (Å)	$3.2 \times 10^{-3} \pm 6 \times 10^{-5}$	$3.5 \times 10^{-3} \pm 8 \times 10^{-5}$	$3.0 \times 10^{-3} \pm 5 \times 10^{-5}$
angles (deg)	0.51 ± 0.01	0.53 ± 0.03	0.51 ± 0.01
improper torsions (deg)	0.97 ± 0.02	1.48 ± 0.02	1.23 ± 0.03
Quality Scores			
van der Waals energy (kcal/mol)[e]	−267 ± 5	−215 ± 5	−246 ± 5
electrostatic energy (kcal/mol)[e]	−2557 ± 35	−2363 ± 18	−2312 ± 20
Ramachandran statistics[f]			
most favored (%)	98.5 ± 0.4	96.6 ± 0.5	97.2 ± 0.7
allowed (%)	1.3 ± 0.4	3.0 ± 0.5	1.8 ± 0.4

	pH 6.6	pH 4.4	pH 1.5
generously allowed (%)	0.0	0.0	0.8 ± 0.5
disallowed (%)	0.0	0.0	0.0
Procheck (ϕ, ψ)[f]	1.2 ± 0.1	0.5 ± 0.2	0.5 ± 0.2
Molprobity Clash[f]	−3.7 ± 0.3	−5.2 ± 0.2	−4.8 ± 0.3
RMSD from the Mean NMR Structure of the α-Helix Monomer Only (Å)[g]			
backbone (C, N, Cα, O)	0.30 ± 0.02	0.28 ± 0.02	0.44 ± 0.03
heavy atoms	0.44 ± 0.02	0.38 ± 0.02	0.67 ± 0.04
RMSD from the Mean NMR Structure of the Dimer (Å)[g]			
backbone (C, N, Cα, O)	0.35 ± 0.02	0.38 ± 0.04	0.54 ± 0.04
heavy atoms	0.50 ± 0.03	0.48 ± 0.04	0.78 ± 0.05
RMSD from the 2ZTA X-ray Structure of the α-Helix Monomer (chain A) Only (Å)[g,h]			
backbone (C, N, Cα, O)	0.51 ± 0.02	0.57 ± 0.02	0.60 ± 0.04
heavy atoms	0.67 ± 0.03	0.93 ± 0.03	0.89 ± 0.05
RMSD from the 2ZTA X-ray Structure of the Dimer (Å)[g,h]			
backbone (C, N, Cα, O)	0.79 ± 0.02	0.73 ± 0.02	0.90 ± 0.04
heavy atoms	1.04 ± 0.05	1.22 ± 0.05	1.38 ± 0.07

[a] All distance and dihedral restraints were included twice, once for each magnetically equivalent monomer chain in the symmetric dimer. Distance restraint groups were compiled using Queen (http://www.cmbi.ru.nl/software/queen).[57]

[b] The range classification is for the intrachain NOEs only. For a discussion of the range classification of the interchain NOEs, see Results.

[c] To maintain H-bond linearity, two restraints (NH–O and N–O) were included for each interaction.

[d] Values are reported as means ± the standard error of the mean. There were no distance restraint violations greater than 0.4 Å or dihedral violations greater than 5°.

[e] Values obtained from ARIA.[34]

[f] Calculated using the Protein Structure Validation Suite (http://psvs-1_5-dev.nesg.org).[58]

[g] Structures were superposed, and RMSDs were calculated using the *align* function of PyMol.[35]

[h] The RMSDs for comparisons between average NMR structures at the different pH values are as follows: pH 6.6 vs pH 4.4 (0.55, 1.21, 0.62, 1.22), pH 4.4 vs pH 1.5 (0.76, 1.22, 0.84 1.28), and pH 6.6 vs pH 1.5 (0.78, 1.36, 1.42, 1.87), where the first number is the backbone comparison for the monomers, the second the heavy atom comparison for the monomers, the third the backbone comparison for the dimers, and the last the heavy atom comparison for the dimers.

Table 2.

Effects of pH on Supercoil Parameters and Ion Pair Distances[a]

	pH 6.6	pH 4.4	pH 1.5	X-ray set[b]
		Crick Supercoil Parameters[c]		
R_0, superhelix radius (Å)	**4.54 ± 0.02**	**4.60 ± 0.02**	**4.75 ± 0.05**	4.84 ± 0.03
R_1, helix radius (Å)	2.16 ± 0.01	2.19 ± 0.01	2.17 ± 0.02	2.13 ± 0.06
ω_0, superhelix frequency (deg/residue)	**−4.78 ± 0.08**	**−3.18 ± 0.11**	**−2.66 ± 0.16**	−3.78 ± 0.07
ω_1 helix frequency (deg/residue)	**102.36 ± 0.09**	**102.17 ± 0.08**	**101.87 ± 0.36**	105.51 ± 1.13
d, rise/residue (Å)	1.494 ± 0.000	1.463 ± 0.002	1.486 ± 0.005	1.54 ± 0.01
Z_{off}, chain axial offset (Å)	0.013 ± 0.002	0.007 ± 0.001	0.010 ± 0.002	0.002 ± 0.003
		Ion Pair Distances (Å) and Fractions of Hydrogen-Bonded Salt Bridges[d]		
intrachain				
E11–K8 (intra)	7.6 ± 0.7 (15%)	7.5 ± 0.4 (0%)	7.5 ± 0.4 (0%)	3.8 ± 0.4 (42%)
E11–K15 (intra)	8.4 ± 0.3 (0%)	7.8 ± 0.4 (0%)	7.0 ± 0.2 (0%)	6.4 ± 1.0 (0%)
E22–R25 (intra)	**4.9 ± 0.6 (50%)**	**6.7 ± 0.5 (0%)**	**5.3 ± 0.5 (5%)**	4.2 ± 0.4 (42%)
interchain				
E20–K15′ (inter)	**4.0 ± 0.3 (55%)**	**6.0 ± 0.4 (5%)**	**7.4 ± 0.4 (0%)**	5.6 ± 0.6 (17%)
E22–K27′ (inter)	**5.2 ± 0.3 (20%)**	**7.0 ± 0.4 (0%)**	**8.2 ± 0.3 (0%)**	3.7 ± 0.2 (25%)

[a] Values that show a consistent trend with pH (increase or decrease) are indicated in bold.

[b] Six X-ray structures of GCN4p crystals grown between pH 8.5 and 6.0, deposited as PDB entries 2ZTA, 1ZII, 1ZIK, 1ZIL, 2AHP, and 4TL1.

[c] Parameters were calculated with the Coiled Coil Crick Parameterization (CCCP) server (http://www.grigoryanlab.org/cccp).[23] Values are reported as means ± the standard error of the mean over the ensemble of 20 NMR structures at each pH.

d The reported distances are the closest approach values between the charged side-chain N and O atoms of the respective ion pairs. For the NMR structures, 50 distances were averaged at each pH (25 NMR structures × 2 monomers). For the X-ray set, 12 distances were averaged (6 X-ray structures × 2 monomers). The value in parentheses gives the percent of structures (NMR and X-ray) in which the stated interaction forms a hydrogen-bonded salt bridge.